

<b>REPORT DOCUMENTATION PAGE</b>			Form Approved OMB NO. 0704-0188		
<small>Public reporting burden for this collection of information is estimated to average 1 hour per response, including the time for reviewing instructions, searching, gathering and maintaining the data needed, and completing and reviewing the collection of information. Send comments regarding this burden estimate or any other aspect of this collection of information, including suggestions for reducing this burden to Washington Headquarters Services, Directorate for Information Operations and Reports, 1215 Jefferson Davis Highway, Suite 1204, Arlington, VA 22202-4302, and to the office of Management and Budget, Paperwork Reduction Project (0704-0188), Washington, DC 20503.</small> <b>PLEASE DO NOT RETURN YOUR FORM TO THE ABOVE ADDRESS.</b>					
<b>1. REPORT DATE (MM-DD-YYYY)</b> MARCH 6, 2002		<b>2. REPORT TYPE</b> FINAL		<b>3. DATES COVERED</b> 06/01/1998 THROUGH 12/31/2001	
<b>4. TITLE AND SUBTITLE</b> An Investigation for Fracture Toughness and Creep Behavior in Carbon Doped Nanocrystalline Nickel			<b>5a. CONTRACT NUMBER</b>		
			<b>5b. GRANT NUMBER</b> N00014-98-1-0666		
			<b>5c. PROGRAM ELEMENT NUMBER</b>		
<b>6. AUTHOR(S)</b> Reza A. Mirshams, Ph.D. - Project Investigator S. H. Whang, Ph.D. Chenghe Xiao Ph.D. W. M. Yin, Ph.D.			<b>5d. PROJECT NUMBER</b>		
			<b>5e. TASK NUMBER</b>		
			<b>5f. WORK UNIT NUMBER</b>		
<b>7. PERFORMING ORGANIZATION NAME(S) AND ADDRESS(ES)</b> Southern University and A & M College, OGSP-Baton Rouge, LA 70813			<b>8. PERFORMING ORGANIZATION REPORT NUMBER</b>		
<b>9. SPONSORING/MENTORING AGENCY NAME(S) AND ADDRESS(ES)</b> OFFICE OF NAVAL RESEARCH (ONR) 800 NORTH QUINCY STREET ARLINGTON, VIRGINIA 22217			<b>10. SPONSOR/MONITOR'S ACRONYM(S)</b>		
<div style="display: flex; justify-content: space-between; align-items: center;"> <div><b>12. DISTRIBUTION/AVAILABILITY STATEMENT</b> UNLIMITED</div> <div style="font-size: 2em; font-weight: bold;">20020702 020</div> </div>					
<b>13. SUPPLEMENTARY NOTES</b> One postdoctoral research associate, two graduate students, and two undergraduate students were supported by this grant. And, two more graduate students are still continuing their research in this area.					
<b>14. ABSTRACT</b> Electrodeposited nanocrystalline nickel that exhibits extraordinary high strength would be a promising candidate for a structural material. The potential engineering applications of nanocrystalline materials need more detailed study on deformation and fracture toughness at room and elevated temperatures under tensile loading. Fracture toughness and creep deformation of nanocrystalline Ni, Ni-C, and Ni-B studied under the course of this research. The results have been published in four (4) papers in refereed journals and have been presented in several international symposiums. One additional manuscript has been submitted recently for publication.					
<b>15. SUBJECT TERMS</b> Tensile behavior and fracture in nickel and carbon doped nanocrystalline nickel, Creep behavior of nanocrystalline nickel at 290 and 373 K, Creep in boron-doped nanocrystalline nickel, R-Curve characterization of the fracture toughness of nanocrystalline nickel thin sheets, Effect of interstitials on tensile strength and creep in nanostructured Ni					
<b>16. SECURITY CLASSIFICATION OF:</b> UNCLASSIFIED		<b>17. LIMITATION OF ABSTRACT</b>	<b>18. NUMBER OF PAGES</b>	<b>19a. NAME OF RESPONSIBLE PERSON</b> DIOLA BAGAYOKO, PH.D.	
<b>a. REPORT</b>	<b>b. ABSTRACT</b>			<b>c. THIS PAGE</b>	<b>19b. TELEPHONE NUMBER (Include area code)</b> (225) 771-2730

# **FINAL REPORT**

The United States Department of Defense  
Office of Naval Research

Grant Number  
N00014-98-1-0666

*An Investigation for Fracture Toughness and Creep Behavior in  
Carbon Doped Nanocrystalline Nickel*

## **Performing Organizations**

Southern University and A & M College  
Baton Rouge, Louisiana

Polytechnic University  
Brooklyn, New York

University of North Texas  
Denton, Texas

**February 2002**

## Summary

Electrodeposited nanocrystalline nickel that exhibits extraordinary high strength would be a promising candidate for a structural material. The potential engineering applications of nanocrystalline materials need more detailed study on deformation and fracture toughness at room and elevated temperatures under tensile loading. Fracture toughness and creep deformation of nanocrystalline Ni, Ni-C, and Ni-B studied under the course of this research. The results have been published in four (4) papers in refereed journals and have been presented in several international symposiums. One additional manuscript has been submitted recently. One postdoctoral research associate, two graduate students, and two undergraduate students supported by this grant and two more graduate students are still continuing their research in this area.

## Table of Contents

Summary

Paper 1

Paper 2

Paper 3

Paper 4

Paper 5 (manuscript)

## Tensile behavior and fracture in nickel and carbon doped nanocrystalline nickel

Chenghe Xiao <sup>a</sup>, R.A. Mirshams <sup>a,\*</sup>, S.H. Whang <sup>b</sup>, W.M. Yin <sup>b</sup>

<sup>a</sup> Department of Engineering Technology, University of North Texas, Denton, TX 76203, USA

<sup>b</sup> Department of Mechanical Engineering, Polytechnic University, Six Metrotech Center, Brooklyn, NY 11201, USA

Received 17 December 1999; received in revised form 3 April 2000

### Abstract

The potential engineering applications of nanocrystalline materials need more detailed study on deformation and fracture mechanisms at room and elevated temperatures under tensile loading. This paper reports results of a series of experiments carried out on nickel and carbon doped nanocrystalline nickel with different carbon concentrations from 500 to 1000 ppm at room temperature to 300°C. Grain growth was observed in nanocrystalline nickels as the testing temperature increases. A fast grain growth was noticed at 300°C. Pure nanocrystalline nickel experienced an abnormal grain growth at 500°C and its tensile properties reduced to a very low level. The addition of carbon exerted a potential effect to enhance the stability of the microstructure in nanocrystalline nickel at intermediate temperatures. However, carbon doped nickels exhibited lower tensile properties. Nanocrystalline nickels displayed a conventional Hall–Petch relationship. The results are discussed in relation to microstructural characteristics by using TEM and SEM. © 2001 Elsevier Science B.V. All rights reserved.

**Keywords:** Nanocrystalline materials; Nickel; Mechanical properties; Grain growth

### 1. Introduction

Nanocrystalline materials have been investigated for a decade [1–4]. The nanocrystalline materials have identical crystal structures, but different grain structures from the counterpart conventional materials. Such a difference in grain structure significantly alters some mechanical properties. Currently, many processing methods and their applications have emerged in the areas of magnetic materials, structural materials, catalysis materials, corrosion and wear materials.

In particular, nanocrystalline materials processed by electrodeposition draw considerable attention due to their advantages in processing and properties: (1) grain sizes between 10 and 100 nm can be controlled easily; (2) the finished products have high density and are porosity-free; and (3) low capital investment for processing is required and consequently, the production cost is low. Recently, this process yielded a number of nanocrystalline alloys which include pure nanocrystalline nickel, Ni–P (less 3000 ppm), Ni–Fe, Ni–Zn, Ni–Mo, Ni–Al<sub>2</sub>O<sub>3</sub>, Ni–SiC, Pd–Ni, etc. [4,5].

Nanocrystalline electrodeposited Ni and Ni–P exhibit excellent mechanical properties potential for structure applications [6,7]. The strength of nanocrystalline nickel sheets far exceeds those of counterpart large grained Ni alloys. The produced nanocrystalline nickel sheets can have an average thickness up to 600 µm.

Preliminary results on the mechanical behavior of electrodeposited nanocrystalline Ni and its alloys showed exceptional strength and ductility at room temperature. As a result, they could be an excellent candidate material for structural application. However, the ultrafine grain structure renders potential problems for applications at intermediate as well as high temperatures due to the abnormal grain growth and grain boundary sliding. Even at room temperature, nanostructured Ni exhibits creep under high stress. One way to resolve these problems is to look into a microalloying approach with carbon and boron.

The carbon and boron addition to Ni–3 (Si, Ti) suppresses the embrittlement in air and distilled water over the whole range of strain rates [8]. This appears

\* Corresponding author. Tel.: +1-940-5654961; fax: +1-940-5652666.

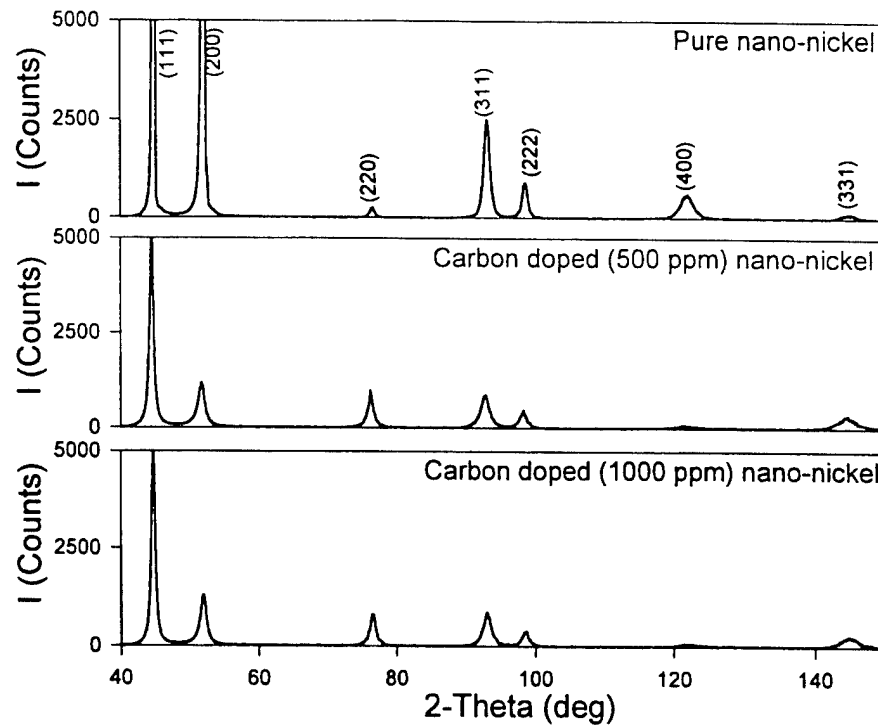


Fig. 1. XRD patterns of as-received nanocrystalline nickels.

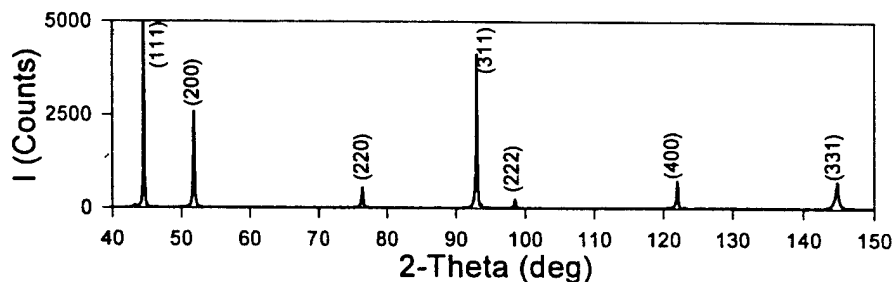


Fig. 2. XRD pattern of a fully annealed pure nanocrystalline nickel (annealed at 800°C for 6 h).

due to the fact that carbon segregates to grain boundaries and alters the fracture mode in these alloys. Both experimental evidence and the first principle calculations on carbon–nickel bonding indicate that carbon could change the character of the grain boundaries in nanocrystalline nickel alloys in a beneficial way. For these reasons, it would be very fruitful to investigate the influence of carbon doping on creep, fracture, strength and grain growth in nanostructured nickel. Second, an excess amount of carbon will form fine carbides along the grain boundaries and in the matrix, which would improve creep resistance in a significant way.

The purpose of this paper is to examine the mechanical properties of pure nanocrystalline nickel and carbon doped nanocrystalline nickel with different amounts of carbon concentration from 500 to 1000 ppm at intermediate temperatures. In addition, grain size effect on ductile to brittle transition and fracture behaviors have been reported.

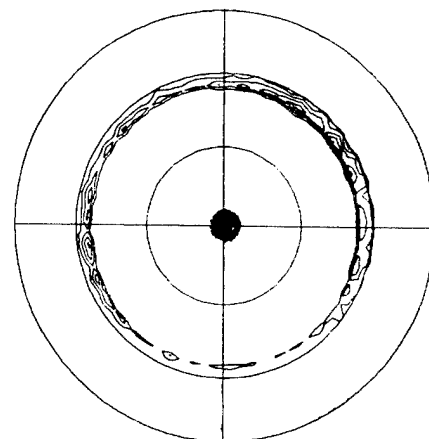


Fig. 3. (111) pole figure of as-received Ni-0C.

Table 1  
Grain size of samples at different temperature holding for 1 h (nm)

Materials	25°C	100°C	200°C	300°C	500°C	800°C
Ni-0C	19	21	25	583	277–2015	8000–26 600
Ni-500C	18	38	48	416		
Ni-1000C	16	38	72	369		

## 2. Experimental procedures

### 2.1. Materials characterization

The materials used in this research were three kinds of nanocrystalline nickels produced by an electrodeposition technique: pure nanocrystalline nickel (designated Ni-0C), 500 ppm carbon doped nanocrystalline nickel (designated Ni-500C) and 1000 ppm carbon doped nanocrystalline nickel (designated Ni-1000C). The materials have full density (pore free) and a narrow grain size range, which has been achieved by the precise control of electrical and chemical parameters [9]. The thickness of the materials is  $\sim 0.3$ – $0.6$  mm. The electrodeposited nanocrystalline materials were acquired from Integran Technologies Inc, Toronto, Canada.

The grain size was determined from the calculation based on the broadening of the X-ray diffraction peaks. The lowest angle peak (111) was chosen for calculation. The X-ray measurements were conducted on a Philips Norelco two-axis diffractometer with Jade analysis software. The crystalline grain size was estimated from the following formula [10]:

$$\text{Grain size} = \{0.9\lambda / \sqrt{[B^2 - b^2]}\} / \cos \theta \quad (1)$$

where  $\theta$  is half of the reported peak centroid,  $B$  is the reported peak width at half maximum in radians,  $b$  is the instrument's broadening and  $\lambda$  is the wavelength.

Scanning electron microscopy (SEM) was used to estimate grain sizes bigger than 100 nm for the samples tested at higher temperatures. A Hitachi SEM was used for this purpose. The etchant for microscopic examination consists of one part  $\text{HNO}_3$  (concentrated) and one part acetic acid. Only fresh solution was used.

The pole figures were obtained from Philips X'Pert MRD four-axis X-ray diffractometer by tilting the specimen in reflection to a maximum of  $90^\circ$  in  $2^\circ$  angular intervals.

### 2.2. Mechanical testing

Dog-bone shaped tensile test samples were water-jet machined to have a nominal gage section of  $25.4 \text{ mm} \times 4 \text{ mm}$ . The tensile tests were carried out on a MTS 810 machine with a maximum 2500-kg load cell and Test-Star™ II control system software. An ATS high temperature extensometer with a gauge length of 25.4 mm

was used. Both load and displacement signals were recorded directly on a PC. The specimen thickness varies from 0.3 to 0.35 mm for pure nickel, 0.37 to 0.5 mm for 500-ppm carbon doped nickel, and 0.45 to 0.59 mm for 1000-ppm carbon doped nickel. The tensile tests were conducted at room temperature (RT), 100, 200 and  $300^\circ\text{C}$  respectively. Before running the test, the specimens were held at the test temperature for 1 h. The

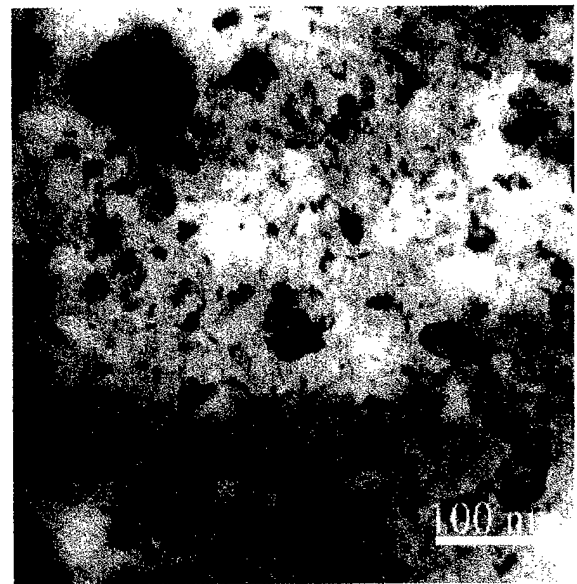


Fig. 4. Typical TEM micrograph (bright field image) of the as-received pure nanocrystalline nickel.

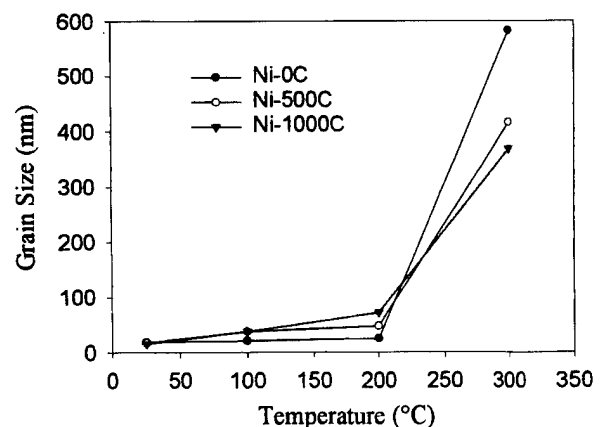


Fig. 5. Variations of grain size as a function of testing temperature for the nanocrystalline nickels.

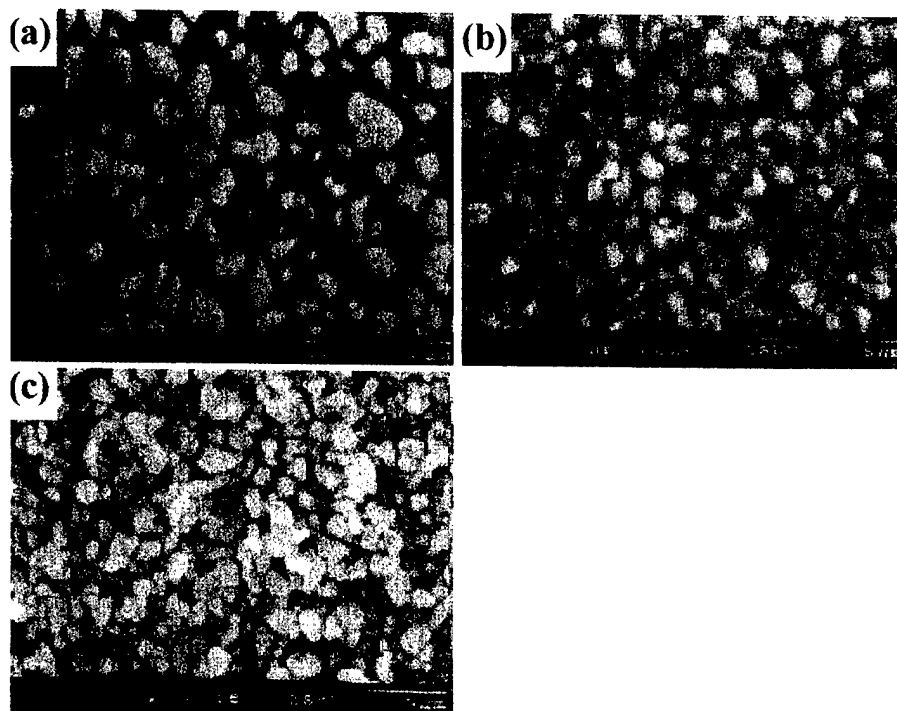


Fig. 6. SEM micrographs of nanocrystalline nickels annealed at 300°C for 1 h. (a) Ni-0C, (b) Ni-500C, and (c) Ni-1000C.

strain rate was kept at  $2 \times 10^{-5} \text{ s}^{-1}$ . The yield strength was defined as the flow stress at a plastic strain of 0.002. Two specimens were tested for each temperature. For comparison and using data in the Hall–Petch plot, some of the pure nanocrystalline nickel specimens were annealed at 100, 200, 300, 500 and 800°C and then tested at room temperature.

### 3. Results and discussions

#### 3.1. Materials characterization

Fig. 1 is the X-ray diffraction patterns of as-received nanocrystalline nickels. For comparison purposes, Fig. 2 shows a X-ray diffraction pattern for a full annealed pure nanocrystalline nickel which illustrates a sharp peak with 56  $\mu\text{m}$  grain size and a random grain orientation.

When comparing the intensities of these nickels, it can be concluded that there are some preferred  $\langle 111 \rangle$  and  $\langle 100 \rangle$  textures in the Ni-0C sample. Further study with X-ray pole figure and phi-scan showed that Ni-0C had weak  $\langle 100 \rangle$  and  $\langle 111 \rangle$  preferred out of plane orientation. From room temperature to 300°C, very slight changes in texture intensities were observed. At 800°C, no texture was found in Ni-0C. There was not any texture in Ni-500C and Ni-1000C materials. Fig. 3 illustrates a (111) pole figure for Ni-0C material.

Comparison of Figs. 1 and 2 indicates that the peaks of as-received nanocrystalline nickel have broaden sig-

nificantly. Grain sizes smaller than 100 nm were decided from calculation based on the peak width. Grain sizes larger than 100 nm were measured from SEM photographs using SigmaScan Pro 4 Image Analysis Software. The measurements are based on the diameter measurement of grains. The grain size is a mean value of at least twenty measurements. Table 1 summarizes grain sizes for the nanocrystalline materials used in this study. A typical TEM micrograph of the as-received Ni-0C is presented in the Fig. 4. Measurement of the grain size of Ni-0C by using TEM micrograph shows the size of grain is  $\sim 18.5 \text{ nm}$ . This is very close to that determined by XRD (19 nm).

To improve the thermal stability of nanocrystalline materials, the traditional approach of grain boundary pinning by solute additions and second phase precipitates is being commonly used. Several studies of the effect of solute additions and second phase precipitates on grain growth have been reported [11–14]. At this study, carbon was used as a solute addition. According to Ni–C binary phase diagram [15], the equilibrium solid solubility of carbon in nickel is negligible up to 800°C. Because the electrodeposition process was conducted at room temperature and nickel is not a carbide forming element, carbide would not form in Ni-500C and Ni-1000C during the processing. Under equilibrium conditions, carbon would preferentially segregate along grain boundaries. A simple calculation suggests that if all the carbon were to segregate along grain boundaries,  $\sim 0.33 \text{ wt.}\%$  of carbon would be required to cover the whole grain boundary area with a



monolayer of carbon atoms. Because the amount of carbon doped in nickel is only 500–1000 ppm (0.05–0.1 wt.%), the grain boundary carbon segregation would be less than a monolayer in extent.

Fig. 5 presents the grain growth rate for all three nanocrystalline nickels. The critical temperatures, for rapid grain growth, at which the materials become unstable are  $\sim 200^\circ\text{C}$ . Under  $200^\circ\text{C}$ , grain growth is very slow and Ni–0C is almost a stable material. However, Ni–1000C shows the best stability among the materials tested above  $300^\circ\text{C}$ . This indicates that trace doped carbon can enhance the thermal stability of nanocrystalline nickel at higher temperatures. Fig. 6 gives SEM micrographs of nanocrystalline nickels annealed at  $300^\circ\text{C}$  for 1 h. It appears that the grain size is more uniform for Ni–1000C material after annealed at  $300^\circ\text{C}$ , Fig. 6(c).

When the Ni–0C samples were annealed at  $500^\circ\text{C}$  for 1 h, a significant abnormal grain growth in some local areas was observed. Abnormal grains appeared as shown in Fig. 7 and their grain sizes are ranged from 12 to  $50\text{ }\mu\text{m}$  compared with that of normal grains in the matrix having values  $0.2\text{--}2\text{ }\mu\text{m}$ . The occurrence of

abnormal grain growth in metals and alloys are generally related to the presence of restraining forces against grain growth [16]. Typical restraining forces are second phase particles, free surface and crystallographic texture. In the present study, the main reason for the abnormal grain growth would be associated to the presence of weak textures. The mechanism of abnormal grain growth in Ni–0C would be related to coalescence of some closely oriented grains. Normally, neighboring grains that have very similar crystal orientation tend to coalesce during the grain growth process. On the other hand, when abnormal grains of significantly different crystal orientations meet each other, coalescence is no longer easy [17]. Fig. 8 shows three cubic grains have inlaid together with a close  $\langle 111 \rangle$  orientation and have grown together.

### 3.2. Mechanical testing

Fig. 9 shows variations of ultimate tensile strength, yield strength and elongation versus testing temperature for nanocrystalline nickels. In the testing temperature range, pure nanocrystalline nickel exhibits better tensile properties than those of carbon doped nickels. Higher carbon contents have reduced most tensile properties (Fig. 9(a,b)). The changes of ultimate tensile strength and yield strength versus temperature are similar for pure and carbon doped nanocrystalline nickels. Both ultimate tensile strength and yield strength decrease with increasing testing temperature. However, the strength decreases much faster with increasing testing temperature for Ni–0C. The strength of Ni–0C is even lower than those of carbon doped nickels when it is tested at  $300^\circ\text{C}$ .

The elongation changes versus testing temperature for the nanocrystalline nickels are presented in Fig. 9(c). The elongation of Ni–0C increases quickly from room temperature to  $200^\circ\text{C}$ . It is observed when testing temperatures further raise to  $300^\circ\text{C}$ , the elongation of Ni–0C sharply declines. This would be an indication of a brittle to ductile transition at  $200\text{--}300^\circ\text{C}$  in Ni–0C material. Although the elongation for carbon doped nanocrystalline nickels are lower than that of Ni–0C in the testing temperature range, the brittle to ductile transition is not observed for the carbon doped nanocrystalline nickels. The brittle to ductile transition temperature for carbon doped nickels might be enhanced to a higher temperature due to the carbon addition. However, the elongation of C500Ni is very close to that of Ni–0C at  $300^\circ\text{C}$ . This observation suggests that the addition of carbon exerts a potential effect to enhance the thermal stability of nanocrystalline nickel.

A Hall–Petch plot of  $\sigma_{0.2}$  yield strength for electrodeposited nanocrystalline nickels from this study and other sources [18,19] is displayed in Fig. 10. Linear fit

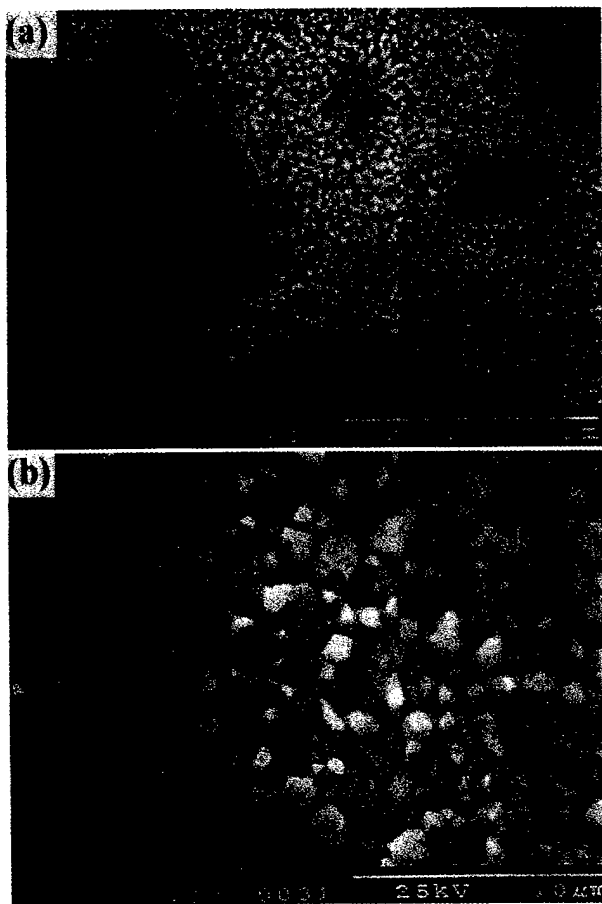


Fig. 7. SEM micrographs of Ni–0C annealed at  $500^\circ\text{C}$  for 1 h. (a) An over view, and (b) a view of small grain area in (a) at a higher magnification.

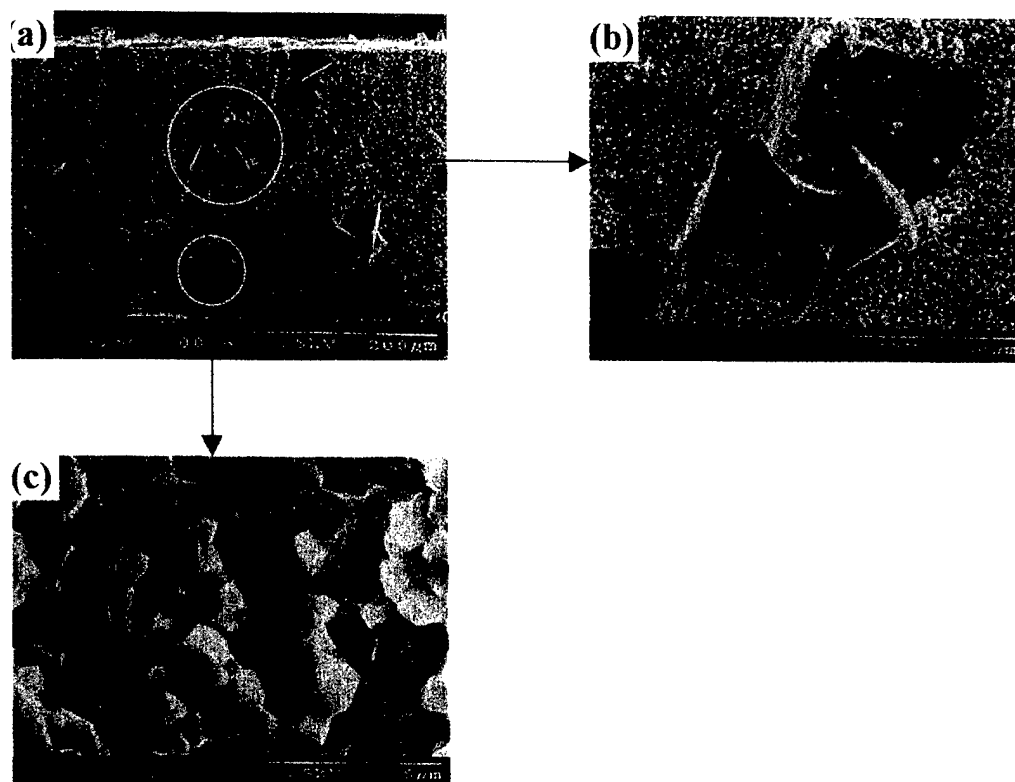


Fig. 8. SEM fractographs of Ni-0C annealed at 500°C. (a) A cross-section overview of fracture surface, (b) a high magnification view of some large grains in (a) and (c) a high magnification view of a small grain area in (a).

with the least squares method was computed for all the data in Fig. 10 and the line shown through the data represents the best fit. Then the Hall–Petch constants were calculated to have the following values:

$$\sigma_0 = 7.0 \text{ MPa}; k = 5665 \text{ MPa nm}^{-1/2}$$

The Hall–Petch equation is presented as the following:

$$\sigma_y = \sigma_0 + kd^{-1/2} = 7.0 + 5665d^{-1/2} \quad (2)$$

with yield strength  $\sigma_y$  measured in MPa and grain size  $d$  measured in nm. It is clear that the electrodeposited pure nickel obeyed a Hall–Petch law all the way in grain size value range from 266  $\mu\text{m}$  to 19 nm. Due to rather low value of  $\sigma_0$ , Eq. (2) predicts that very low strength will be expected if electrodeposited pure nickel sheets would have relatively large grains. Nieh and Wadsworth [20] pointed out that the Hall–Petch relation holds in materials with grain sizes over a critical value. When the grain size is below the critical value, hardness may decrease with decreasing grain size. For grain size of pure nickel, the critical value has been estimated to be 2.5 nm [13]. Thus, the grain sizes of the electrodeposited pure nickels in this research satisfy the above range very well (Fig. 10).

Fig. 11 shows that Ni-0C sheet exhibits a typical

ductile fracture mode when tested from room temperature to 200°C. A transgranular-tearing mode is prevalent for the specimen tested at room temperature. For Ni-0C tested at 100°C and 200°C, the fracture surface exhibits more ductile fracture features. The material separates by transgranular microvoid processes or dimple mode fracture (Fig. 11(b,c)). When Ni-0C sheet is tested at 300°C, a mixed fracture mode is observed with both transgranular ductile fracture and transgranular brittle fracture. A large decrease in strength and ductility occurs simultaneously with the introduction of a transgranular brittle fracture mode at this testing temperature (Fig. 9 and Fig. 11(d)).

In order to determine the effect of prior annealing on the tensile properties at room temperature, some Ni-0C specimens were first annealed at 100, 200, and 300°C. Samples annealed at or below 200°C, their failure modes are still ductile fracture mode (Fig. 12(a,b)). When the samples annealed at 300°C, the fracture mode becomes a brittle fracture. This fracture feature is dominated by intergranular fracture with a small amount of transgranular brittle fracture (Fig. 12(c)). Its ultimate strength is only  $\sim 400$  MPa. When the Ni-0C sample is annealed at 500°C, the fracture mode becomes totally intergranular fracture. Fig. 8

clearly indicates that the separation is from the grain boundary in both big and small grain areas. The ultimate strength is only about 100 MPa in this case. When the Ni-0C is further annealed at 800°C, the ultimate strength is just reduced to a few tens MPa. This indicates that when Ni-0C material is annealed at or above 300°C, brittllization occurs and it could be mainly associated to the grain boundary weakening due to the grain growth. Meanwhile, when the samples are annealed at higher temperatures (above 500°C), the weakness could be associated to the abnormal grain growth. Although grain growth will reduce the strength, it seems that the loss of strength would be mainly related

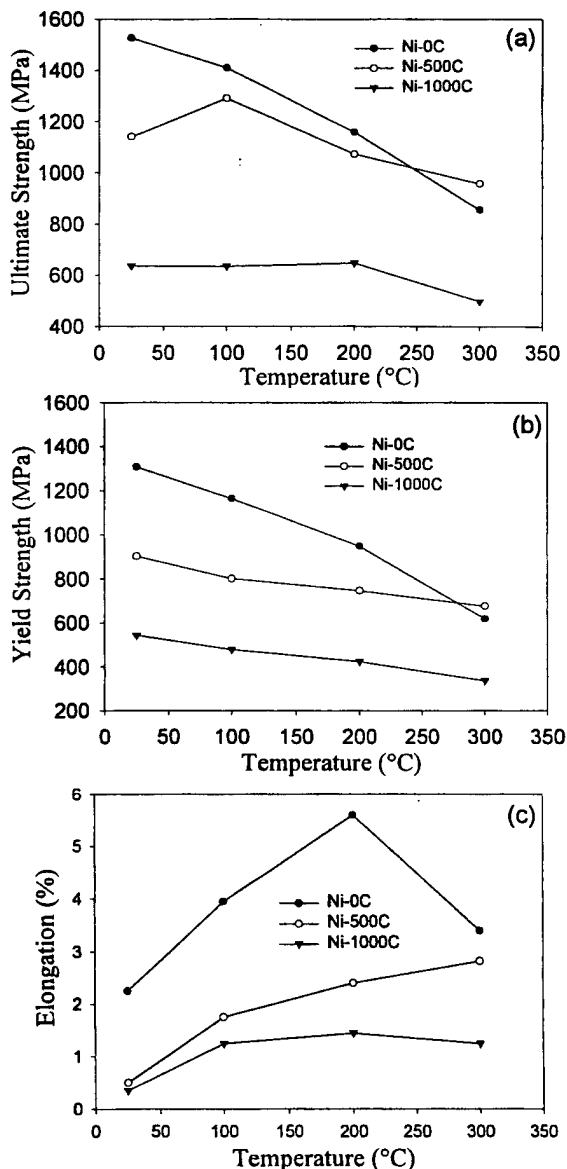


Fig. 9. Mechanical properties as a function of testing temperatures for the nanocrystalline nickels. (a) Ultimate strength, (b) yield strength and (c) elongation.

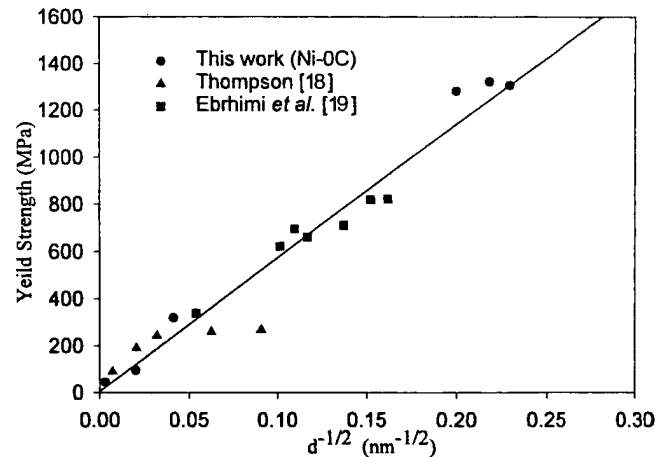


Fig. 10. Hall-Petch plot of yield strength for nanocrystalline nickel and normal grain size nickel.

to the grain boundary weakening effect in the materials examined. However, further investigation on the grain boundary characterizations is required for more definite conclusions.

#### 4. Conclusions

(1) Grain growth was observed in pure and carbon doped nanocrystalline nickels. From room temperature to 200°C, the grains grow very slowly and the grain size is still under 100 nm. At 300°C, nanocrystalline nickels experienced a fast grain growth. The rate is higher for Ni-0C.

(2) Annealed at 500°C, Ni-0C exhibited an abnormal grain growth.

(3) The tensile properties of carbon doped nanocrystalline nickel reduced with the addition of carbon from 500 to 1000 ppm. The more carbon doped, the lower the tensile properties.

(4) Above 300°C, Ni-500C exhibited a higher strength than that of Ni-0C. The addition of carbon exerted a potential effect to enhance the thermal stability of nanocrystalline nickel at intermediate temperature.

(5) Nanocrystalline nickels exhibited a conventional Hall-Petch relationship.

#### Acknowledgements

The authors would like to thank Dr Lawrence Kaba-coff at the Office of Naval Research for financial support to complete this research under grant N00014-98-1-0666.

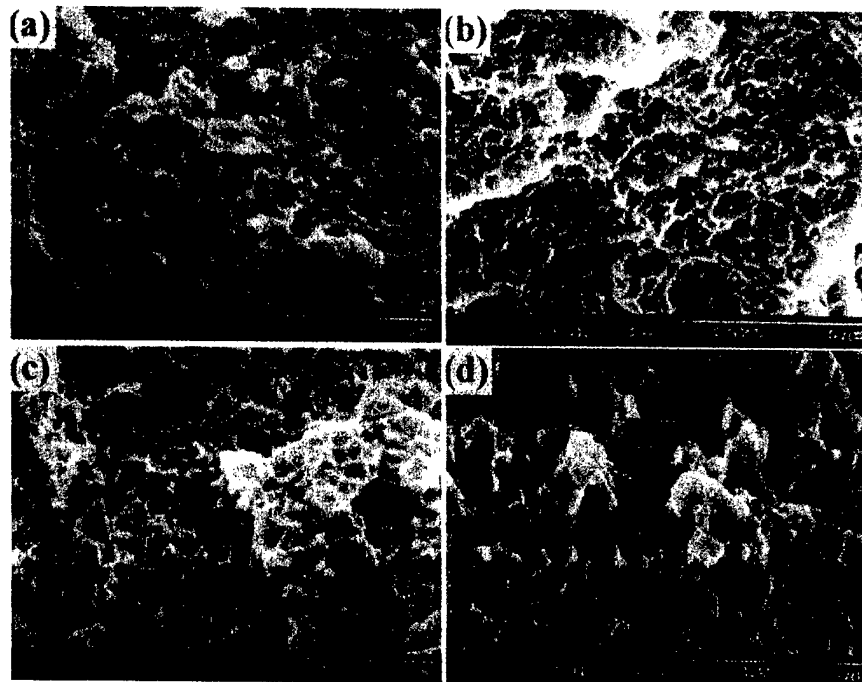


Fig. 11. SEM fractographs of Ni-0C tested at different temperatures. (a) Room temperature, (b) 100°C, (c) 200°C and (d) 300°C.

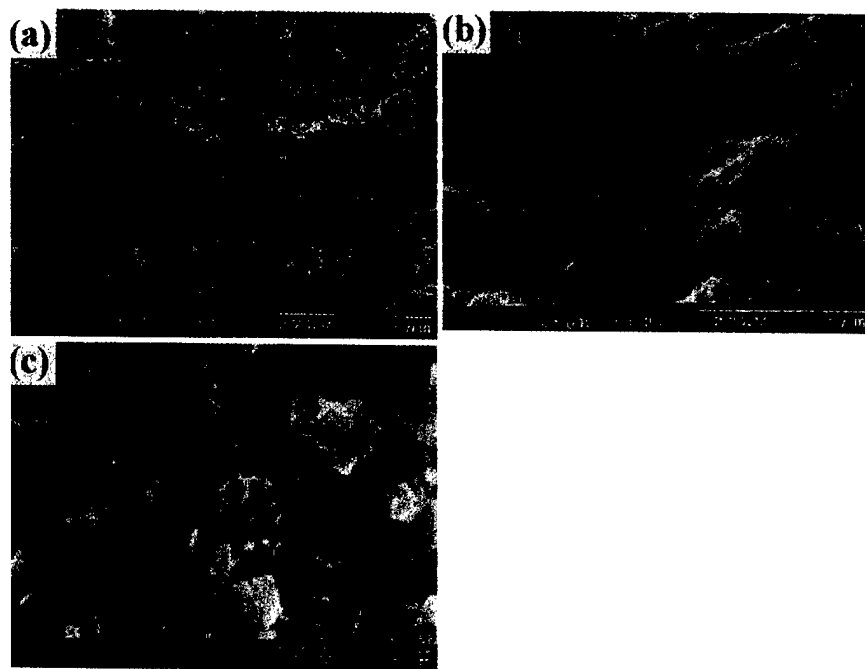


Fig. 12. SEM fractographs of Ni-0C annealed at different temperatures and then tested at room temperature. (a) Annealed at 100°C, (b) annealed at 200°C, and (c) annealed at 300°C.

## References

- [1] H. Gleiter, *Prog. Mater. Sci.* 33 (1989) 223.
- [2] K.T. Aust, U. Erb, G. Palumbo, in: S.J. Singh, F.H. Froes (Eds.), *Processing and Properties of Nanocrystalline Materials*, The Minerals, Metals and Materials Society, Warren, PA, USA, 1996, p. 11.
- [3] C. Cheung, D. Wood, U. Erb, in: S.J. Singh, F.H. Froes (Eds.), *Processing and Properties of Nanocrystalline Materials*, The Minerals, Metals and Materials Society, Warren, PA, USA, 1996, p. 479.
- [4] C. Suryanarayana, F.H. Froes, *Metall. Trans. A* 23A (1992) 1071.
- [5] C. Cheung, G. Palumbo, U. Erb, *Scripta Metall.* 31 (1994) 735.
- [6] A.M. El-Sherik, U. Erb, J. Page, *Surf. Coatings Technol.* 88 (1996) 70.
- [7] U. Erb, G. Palumbo, R. Zugic, K.T. Aust, in: S.J. Singh, F.H. Froes (Eds.), *Processing and Properties of Nanocrystalline Materials*, The Minerals, Metals and Materials Society, Warren, PA, USA, 1996, p. 479.

- rials, The Minerals, Metals and Materials Society, Warren, PA, USA, 1996, p. 93.
- [8] T. Takasugi, S. Hanada, *Mater. Sci. Eng.* A193 (1995) 407.
- [9] A.M. Alfantazi, J. Page, U. Erb, *J. Appl. Electrochem.* 26 (1996) 1225.
- [10] Software Jade 3.1 Manual, Long Beach, CA, USA, 'XRD Pattern Processing for the PC', Materials Data, Inc., Long Beach, CA, USA, 1997.
- [11] B. Gunther, A. Kumpmann, H.D. Kunze, *Scripta Metall. Mater.* 27 (1992) 833.
- [12] K. Lu, W.D. Wei, J.T. Wang, *J. Appl. Phys.* 69 (1991) 7345.
- [13] K. Boylan, D. Ostrander, U. Erb, G. Palumbo, K.T. Aust, *Scripta Metall. Mater.* 25 (1991) 2711.
- [14] S.C. Mehta, D.A. Smith, U. Erb, *Mater. Sci. Eng.* A204 (1995) 227.
- [15] H. Baker, H. Okamoto (Eds.), *Alloy Phase Diagrams*, vol. 3, ASM International, Materials Park, Ohio, 1992, p. 112.
- [16] P. Cotterill, P.R. Mould, *Recrystallization and Grain Growth in Metals*, Wiley, New York, 1976, p. 305.
- [17] Y.B. Chun, S.K. Hwang, S.I. Kwun, M.H. Kim, *Scripta Mater.* 40 (1999) 1165.
- [18] A.W. Thompson, *Acta Metall.* 23 (11) (1975) 1337.
- [19] F. Ebrahimi, G.R. Bourne, M.S. Kelly, T.E. Matthews, *Nanostruct. Mater.* 11 (3) (1999) 343.
- [20] T.G. Nieh, J. Wadsworth, *Scripta Metall. Mater.* 25 (1991) 955.

## Creep behavior of nanocrystalline nickel at 290 and 373 K

W.M. Yin <sup>a,\*</sup>, S.H. Whang <sup>a</sup>, R. Mirshams <sup>b</sup>, C.H. Xiao <sup>b</sup>

<sup>a</sup> Department of Mechanical Engineering, Polytechnic University, Six Metrotech Center, Brooklyn, NY 11201, USA

<sup>b</sup> Department of Mechanical Engineering, Southern University and A&M College, P.O. Box 9987, Baton Rouge, LA 70813, USA

Received 13 December 1999; received in revised form 20 April 2000

### Abstract

The uniaxial tensile creep behavior of porosity-free nanocrystalline nickel with 30 nm grains produced by an electrodeposition processing has been investigated under constant and step-load conditions at room temperature and 373 K in a load range 500–1050 MPa. The experimental results showed that significant creep deformation occurred even at room temperature at an initial applied stress of 600 MPa or higher. The creep resistance was very sensitive to test temperature. The grain size and microstructure of the as received and post-creep specimens have been characterized by conventional TEM techniques. An attempt has been made to explain the deformation behavior and creep mechanisms based on current findings. © 2001 Elsevier Science B.V. All rights reserved.

**Keywords:** Nanocrystalline material; Nickel; Creep; Mechanical properties

### 1. Introduction

Nanocrystalline materials exhibit unique mechanical, chemical, electronic as well as magnetic properties [1–4]. As a result, considerable interest concerning these materials has been shown among scientists and engineers in recent years. Nevertheless, the majority of the research work on nanocrystalline materials has been limited to simple measurements such as hardness tests and compression tests due to the unavailability of large-scale fully-dense bulk nanocrystalline materials. Creep behavior of some nanocrystalline metals and alloys produced by different processing techniques [5–7] have been investigated in the past. The steady state creep rate of nano-copper with a grain size of 30 nm is linearly proportional to the effective stress [5]. The activation energy for creep which was obtained from the plot of the threshold stress versus  $1/T$  was found to be 0.72 eV. This value 0.72 eV is similar to that of the grain boundary diffusion in a coarse-grained nickel, 1.08 eV [8], but deviates from that of the lattice diffusion, 2.0 eV. The preliminary studies suggest that grain

boundary diffusion creep is dominant in a nanocrystalline Ni–P alloy (28 nm) [6] and Y-SZP ceramics (40 nm) [7], whereas the power law mechanism controls creep in an Al–Mg alloy of submicrometer grain size [9].

Nano-nickel is one of the nanocrystalline metals that have been subjected to extensive scientific investigations in the areas of grain growth kinetics [10,11] and mechanical behavior [12,13]. In nanocrystalline nickel, the grain size effect on yield strength was interpreted in terms of the Hall–Petch (H–P) relation down to a grain size of 10 nm [12,13], whereas a negative H–P slope was observed below a grain size of 10 nm [12]. It was suggested that dynamic creep might be responsible for the observed deviation from the H–P relation in the absence of strain hardening. Such results of short-term creep tests in nanocrystalline nickel suggest an important role of grain boundary sliding and diffusion in the primary creep [12]. It is also important to understand the steady stage creep and its mechanism at/near room temperature in this material. In this paper, we will report the experimental results on creep behavior of this material at room temperature and 373 K. A brief discussion has been made regarding the deformation mechanisms of nanocrystalline nickel.

\* Corresponding author.

E-mail address: wyin01@utopia.poly.edu (W.M. Yin).

## 2. Experimental procedure

The sheets of pure nanocrystalline nickel were prepared by pulse electrodeposition technique [14] by Integran Technologies Inc., Toronto, Canada. The material had a nominal thickness of 0.3 mm and was fully dense with a narrow grain size range. Tensile and creep specimens with 15-mm gauge length and 3 mm gauge width were cut by an electron-discharge machine (EDM). The tensile tests were carried out on an MTS-810 Material test system under stroke control condition at the initial strain rates of  $4 \times 10^{-5}$  and  $8 \times 10^{-4} \text{ s}^{-1}$ . A high sensitivity extensometer was attached to the gauge section of the specimens to measure displacement. Both load and displacement signals were digitized by 195 A Keithley digital multimeters and recorded using an IBM PC with an IEEE-480 board.

The uniaxial creep tests were performed at room temperature and 373 K in the load range of 500–1050 MPa using a Satec M3 creep machine. The step-load method was employed to exploit creep strain rate change and instantaneous behavior during loading and unloading. TEM foils were cut by EDM from the as received sheets as well as from the deformed specimens. The final polishing was prepared by double-jet electropolishing in a solution of 25%  $\text{HNO}_3$  and 75%  $\text{CH}_3\text{OH}$  at 220 K and 30 V. The X-ray line broadening technique was used to determine the average grain size. TEM bright and dark field images have been employed to characterize the microstructure of as received material and post-creep samples.

## 3. Results

### 3.1. Tensile tests

The room temperature tensile tests showed a sharp increase in strength of nanocrystalline nickel as compared with that of polycrystalline nickel of 30  $\mu\text{m}$  grain size, as shown in Fig. 1a. The 0.2% offset engineering strength increased from 300 MPa, in polycrystalline nickel, to 1.0 GPa in its nanocrystalline counterpart. The ultimate strength was 1.5 GPa in nanocrystalline nickel. On the other hand, a significant reduction in ductility from that of polycrystalline nickel is seen, i.e. the elongation at a strain rate of  $4 \times 10^{-5} \text{ s}^{-1}$  was as low as 4% in nanocrystalline nickel. In addition, the tensile strength is sensitive to strain rate (Fig. 1a). The higher the strain rate is, the higher the yield strength becomes. The testing temperature can significantly influence tensile behavior even within ambient temperature range. The yield strength at 373 K dropped by 25% compared with that at room temperature (Fig. 1b).

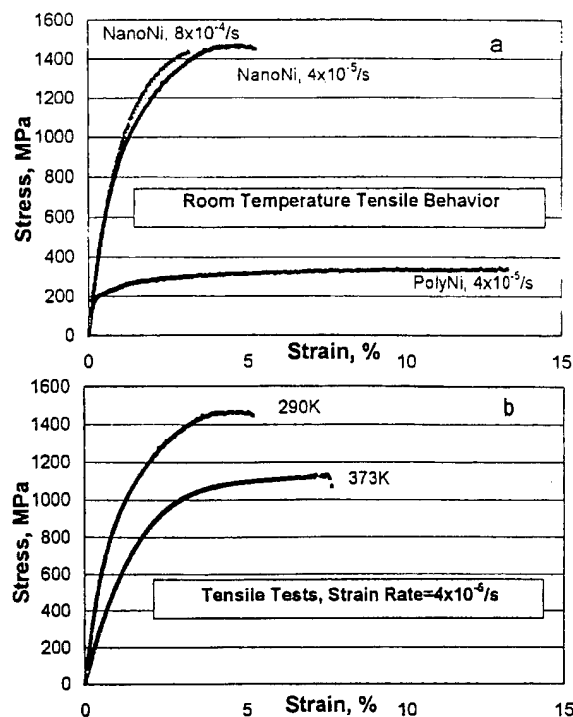


Fig. 1. Tensile behavior at room temperature and 373 K, (a) strain rate dependence, (b) temperature dependence.

### 3.2. Creep behavior

After prolonged primary creep, the creep rate at 600 MPa decreased to  $9 \times 10^{-10} \text{ s}^{-1}$  at minimum, which is near the measurable limit. It is important to note that the primary creep lasted more than 200 h at 600 and 700 MPa, but it decreased to 130 h at 900 MPa (Fig. 2). Although the applied stress was close to the yield strength, the creep rate was very small in nanocrystalline nickel at room temperature. Therefore, the creep tests at room temperature were interrupted at low loads or adjusted to higher loads when the minimum strain rate was achieved. After the load was decreased from 1050 to 800 MPa, a prolonged incubation period more than 60 h was observed, as shown in Fig. 3.

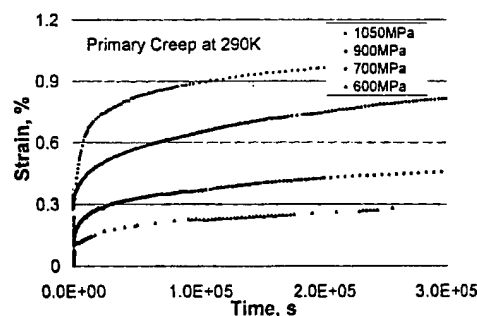


Fig. 2. Primary creep of nanocrystalline nickel at room temperature.

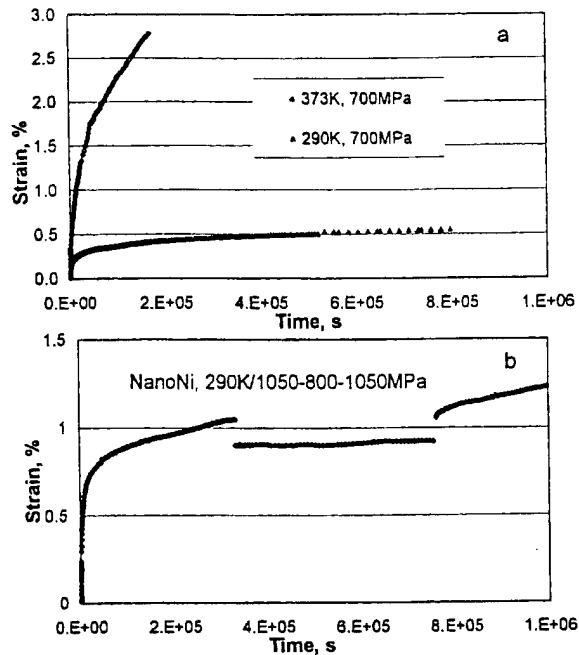


Fig. 3. Tensile creep curves of nanocrystalline nickel, (a) 700 MPa, (b) Step-load.

Nanocrystalline nickel exhibited an accelerated creep deformation at 373 K where the creep rate at 700 MPa reached a minimum value  $8.8 \times 10^{-8} \text{ s}^{-1}$ , which is about two order of magnitude larger than that ( $1.1 \times 10^{-9} \text{ s}^{-1}$ ) at room temperature. The decrement load test from 600 to 500 MPa did not show any evidence of such an incubation phenomenon.

### 3.3. Microstructure

The TEM observation shows that the as received material has equiaxed grains with an average size of about 30 nm (Fig. 4). The grain size that was determined by TEM was consistent with the results obtained by an X-ray line broadening method. The specimens from the room temperature creep tests were investigated by TEM and did not show any grain growth. On the other hand, the post-creep specimens that had been tested at 373 K show a slight increase in grain size, observed by TEM.

## 4. Discussion

### 4.1. Tensile deformation

The tensile stress-strain curves for nanocrystalline nickel did not show any linear elastic region. Nevertheless, at a strain rate of  $8 \times 10^{-4} \text{ s}^{-1}$ , a slope of 150 GPa was obtained from the tensile curve at room

temperature in the stress range 200–800 MPa, which is somewhat lower than the Young's modulus of polycrystalline nickel 200 GPa. The strain-stress curve obtained at a strain rate of  $4 \times 10^{-5} \text{ s}^{-1}$  yielded a lower value than that at a strain rate of  $8 \times 10^{-4} \text{ s}^{-1}$ . This indicates that the deformation is sensitive to the strain rate, which implies the existence of time-dependent deformation. Furthermore, with increasing temperature, the strain rate dependence becomes more pronounced.

A nanocrystalline material may be regarded as a composite consisting of crystalline components and intercrystalline components. The portion of the intercrystalline components in polycrystalline materials is so small that its effect on deformation at ambient temperature is negligible whereas in nanocrystalline materials, not only do grain boundaries play an important role, but also triple lines and quadruple nodes might be contributing significantly to deformation. Therefore, the strain in this material may be expressed as:

$$\epsilon = \epsilon_{cl} + \epsilon_{dg} + \epsilon_{gs} \quad (1)$$

The term  $\epsilon_{cl}$  is elastic deformation of crystalline components, equaling  $\sigma/E$ , where  $E$  is Young's modulus. The terms  $\epsilon_{dg}$  and  $\epsilon_{gs}$  are strain from dislocation glide, and strain from grain boundary sliding. From the conventional dislocation theory, the approximate critical repulsive force of a single dislocation against a grain boundary obstacle in a grain size  $d_0$  can be calculated as follow [16]:

$$\sigma_c = \frac{G}{\pi(1-\nu)} \frac{b}{d_0} \quad (2)$$

In this formula,  $\sigma_c$  is critical stress for moving single straight dislocation,  $d_0$  grain size,  $b$  Burger vector,  $G$  and  $\nu$  are the shear modulus and Poisson's ratio. This means that dislocations can move only when the ap-

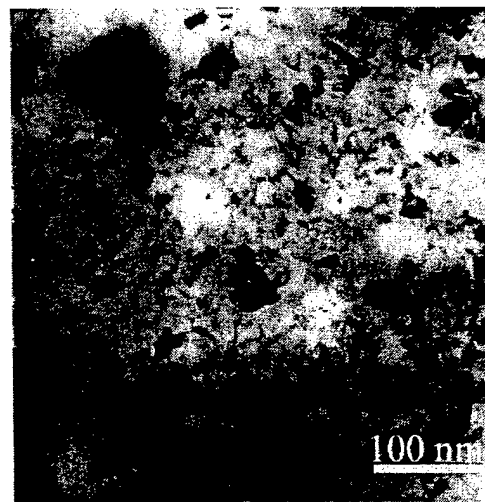


Fig. 4. Microstructure of as received nanocrystalline nickel.



plied stress exceeds the critical repulsive force for a given grain size  $d_0$ . Given the ultrafine grain size  $d_0 = 30$  nm,  $G = 76$  GPa,  $\nu = 0.3$  and  $b = 0.25$  nm, the critical stress  $\sigma_c = 300$  MPa was obtained from the above Eq. (2). When an array of dislocations in a grain is subjected by an applied stress ( $\sigma_a$ ), the lead dislocation near the grain boundary will be subjected to a stress given by an expression [17]:

$$\tau_b = \sum_{j=1}^n \frac{Gb}{2\pi(1-\nu)(l_i - l_j)} \quad (3)$$

In this formula,  $l_i$  ( $l_j$ ) is the distance from dislocation  $i$  ( $j$ ) to the obstacle. The solution showed that the stress acting (back stress) on the lead dislocation near the grain boundary with  $n$  parallel dislocations was found to be approximately 450 MPa for  $n=2$ , 825 MPa for  $n=3$  and 1250 MPa for  $n=4$ , respectively. The stress for four dislocations is higher than the yield stress, 1.0 GPa and therefore, any significant pile-up of dislocations is practically excluded in most grains except much larger grains. It is also true that the grain size distribution exists in this material, and therefore the average grain size can not be used for dislocation pile-up calculations. In larger grains, a dislocation pile-up may occur at a much lower stress level whereas dislocation nucleation may not occur in sufficiently smaller grains. If this is the case, a new question arises as to the source of plastic deformation beyond yield stress. The idea is that the grain boundary migration is a competing mechanism against dislocation mechanism. The grain boundary migration may be carried out by a few plausible mechanisms. First, in the absence of lattice dislocation activity, the activity of grain boundary dislocations would be a logical subject to investigate relative to the other deformation mechanisms in nanocrystalline nickel. By comparing the stress unlocking the Frank–Read source  $\sim Gb/2l$  and the plasticity yield stress  $\sim Kl^{1/2}$  [18], the critical grain size for generation of grain boundary dislocations was estimated to be several nanometers. The stress-induced and original grain boundary dislocations might be expected to travel along the interface without penetrating the nanocrystalline volumes. For the coincidence site lattice model, the Burgers vectors of secondary grain boundary dislocations are only a fraction of those of lattice dislocations. This means that the critical stress for the migration of secondary grain boundary dislocations is much lower than that for the migration of lattice dislocations. Therefore, grain boundary dislocations could be active in nanocrystalline nickel and contribute to plastic deformation. It is not easy to identify dislocations in nano-grains since many deformation dislocations of high energy may be removed during preparation of thin TEM specimens. Second, when the grain boundary structure is disordered and its viscosity lies below a critical value where the viscous

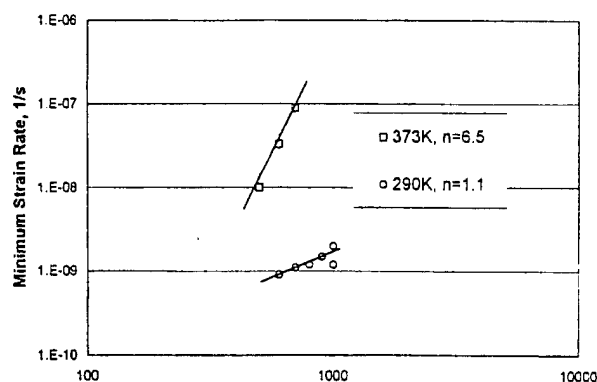


Fig. 5. Minimum strain rate dependent on stress.

flow can occur under the applied stress, the viscous flow may be realized. The viscous flow mode may require thermal activation. The first and second modes may be capable of deforming material under static deformation testing. The relationship between stress and strain rate in viscous flow obeys  $\sigma = 3\eta\dot{\epsilon}$  [15], and viscosity is sensitive to temperature and lesser degree, to applied stress. Third, the material still can be deformed by grain migration mainly caused by diffusion. This mechanism has been well known to occur in polycrystalline metals and alloys at relatively high temperatures. It has been suggested that there is no hardening effect in nanocrystalline materials at room temperature deformation [2,12]. This indicates that the dislocation pile-ups necessary for strain hardening may be absent or negligible in this material. Consequently, the grain boundary migration is the main mechanism for plastic deformation in such a material.

#### 4.2. Creep mechanism

In order to investigate the stress dependence of creep deformation, a plot of strain rate versus stress was made based on constant load and step-load tests (Fig. 5). The stress exponent in Fig. 5 is unity for room temperature creep while it is 6.5 for creep at 373 K. The grains were stable up to 353 K while the nucleation and abnormal grain growth may take place at 393 K [11]. In current experiments, no evident grain growth was found up to 373 K.

The creep rate of diffusional Nabarro–Herring or Coble creep exhibits linear dependence on true applied stress. The dislocation creep rate is practically independent of grain size, while the diffusional creep rate is inversely proportional to the second power of mean grain diameter when the diffusion mass transport occurs via the lattice, and to the third power of mean grain diameter when it occurs through grain boundaries.

At low homologous temperatures and small mean grain diameters, the grain boundary diffusion dominates over the lattice diffusion. Consequently, under these conditions, the diffusional creep will occur by stress directed mass transport through grain boundaries. Assuming spherical grains, Coble derived the following equation for creep rate [19]:

$$\dot{\epsilon} = \frac{148}{\pi} \frac{D_{b0} \delta_b \sigma \Omega}{d^3 k T} \exp\left(\frac{Q_b}{RT}\right) \quad (4)$$

In the formula,  $D_{b0}$  is the grain boundary diffusion coefficient,  $\delta_b$  the effective grain boundary width and  $\Omega$  is the atomic volume. Since diffusion coefficient  $D_{b0}$  in nanocrystalline nickel is not available, the data for polycrystalline nickel, i.e.  $\delta_b D_{b0} = 4 \times 10^{-15} \text{ m}^3 \text{ s}^{-1}$  and  $Q_b = 108 \text{ kJ mol}^{-1}$  [20] were used here. Given  $\Omega = 8.0 \times 10^{-3} \text{ nm}^3$ ,  $d = 30 \text{ nm}$ ,

$$\dot{\epsilon} = \frac{4 \times 10^3 \sigma}{T} \exp\left(-\frac{12996}{T}\right) \quad (5)$$

At room temperature and 700 MPa, the calculated minimum strain rate  $3.3 \times 10^{-10} \text{ s}^{-1}$  is of the same order of magnitude as the experimental value  $11 \times 10^{-10} \text{ s}^{-1}$ . On the other hand, the stress exponent of 6.5 was obtained from the curves of minimum strain rate and stress at 373 K. In addition, the calculated strain rate based on Eq. (4) was much smaller than that of the experimental value at 373 K. This indicates that the creep mechanism may no longer be governed by the Coble mechanism, but possibly by the dislocation mechanism. A detailed investigation is required to elucidate the mechanism.

## 5. Summary

Fully-dense nanocrystalline nickel exhibited a UTS as high as 1.5 GPa. The tensile behavior is sensitive to test temperature and strain rate, probably due to the sliding of intercrystalline components. Creep deformation at room temperature appears to be dominated by a Coble creep mechanism, in which enhanced diffusion along intercrystalline components including grain boundaries, triple junctions and quadruple nodes control the mass transport process. The calculated creep rate at room temperature, based on the Coble creep mechanism, is in agreement with the experimental results. Nevertheless, the creep deformation mechanism

might change from a diffusion-controlled process at room temperature to multiple mechanisms at 373 K. Above ambient temperature, lattice dislocation gliding and grain boundary sliding may play an important role in deformation, though a dominant mechanism has not yet been identified.

## Acknowledgements

The authors wish to thank Dr Lawrence Kabacoff at the Office of Naval Research for financial support of this project. We thank valuable comments of Professor Hans Conrad, North Carolina State University on grain boundary deformation.

## References

- [1] H. Gleiter, *Prog. Mater. Sci.* 33 (1989) 223.
- [2] V.G. Gryaznov, L.I. Trusov, *Prog. Mater. Sci.* 37 (1993) 289.
- [3] C.C. Koch, D.G. Morris, K. Lu, A. Inoue, *MRS Bull.* 2 (1999) 54.
- [4] J.R. Weertman, D. Farkas, K. Hemker, H. Kung, M. Mayo, R. Mitra, H. Van Swygenhoven, *MRS Bull.* 2 (1999) 44.
- [5] B. Cai, Q.P. Kong, L. Lu, K. Lu, *Scr. Mater.* 41 (7) (1999) 755.
- [6] D.L. Wang, Q.P. Kong, J.P. Shui, *Scr. Metall. Mater.* 31 (1) (1994) 47.
- [7] F. Gutierrez-Mora, A. Dominguez-Rodriguez, M. Jimenez-Melendo, *Nanostruct. Mater.* 11 (4) (1999) 531.
- [8] W. Dickenschied, R. Birringer, H. Gleiter, O. Kanert, B. Michel, B. Gunther, *Sol. Stat. Commun.* 79 (1991) 683.
- [9] R. Hayes, V. Tellkamp, E. Lavernia, *Scr. Mater.* 41 (7) (1999) 743.
- [10] N. Wang, Z.R. Wang, K.T. Aust, U. Erb, *Acta Mater.* 45 (4) (1997) 1655.
- [11] U. Klement, U. Erb, A.M. El-Sherik, K.T. Aust, *Mater. Sci. Eng. A203* (1995) 177.
- [12] N. Wang, Z.R. Wang, K.T. Aust, U. Erb, *Mater. Sci. Eng. A237* (1997) 150.
- [13] F. Ebrahimi, G.R. Bourne, M.S. Kelly, T.E. Matthews, *Nanostruct. Mater.* 11 (3) (1999) 343.
- [14] A.M. Alfantazi, J. Page, U. Erb, *J. Appl. Electrochem.* 26 (1996) 1225.
- [15] T.H. Courtney, *Mechanical Behavior of Materials*, McGraw-Hill, New York, 1990.
- [16] T.G. Nieh, J. Wadsworth, *Scr. Metall. Mater.* 25 (1991) 955.
- [17] E. Smith, in: F.R.N. Nabarro (Ed.), *Dislocation in Solids*, vol. 4, 1979, p. 374.
- [18] A. Lasalmonie, J.L. Strudel, *J. Mater. Sci.* 21 (1986) 1837.
- [19] R.L. Coble, *J. Appl. Phys.* 34 (1963) 1679.
- [20] I. Kaur, W. Gust, L. Kozma, *Handbook of Grain and Interphase Boundary Diffusion Data*, Ziegler Press, Stuttgart, 1989.



PERGAMON

Scripta mater. 44 (2001) 569–574



www.elsevier.com/locate/scriptamat

## CREEP IN BORON-DOPED NANOCRYSTALLINE NICKEL

W.M. Yin and S.H. Whang

Department of Mechanical Engineering, Polytechnic University, Six Metrotech Center,  
Brooklyn, NY 11201, USA

(Received August 4, 2000)

(Accepted in revised form September 26, 2000)

*Keywords:* Nanocrystalline nickel; Creep; Tensile strength; Boron doping

### 1. Introduction

Nanocrystalline nickel (nano-nickel) exhibits unique deformation behavior at/near ambient temperatures, which include high tensile strength, limited ductility and room temperature creep. In particular, the creep of this material at/near ambient temperature has drawn considerable attention among scientists. The origin of such creep appears to be associated with grain boundary migration and sliding [1–4]. The majority of creep tests have been carried out with some nanocrystalline metals and alloys produced by electroplating in the past [5,6,7]. The steady state creep rate of nano-copper with a grain size of 30nm is linearly proportional to the effective stress [6]. The activation energy for creep which was obtained from the plot of the threshold stress vs.  $1/T$  was found to be 0.72 eV. This value 0.72 eV is similar to that of the grain boundary diffusion in a coarse-grained copper, 1.08 eV, but far smaller than that of the lattice diffusion, 2.0 eV [8]. The preliminary studies suggest that grain boundary diffusion creep is dominant in a nanocrystalline Ni-P alloy (28nm) [9] and Y-SZP ceramics (40nm) [10], whereas the power law mechanism controls creep in an Al-Mg alloy of submicrometer grain size [11].

Nano-nickel has been subjected to extensive scientific investigations in the areas of grain growth kinetics [12,13] and mechanical behavior [5,14]. In nano-nickel, the grain size effect on yield strength was interpreted in terms of the Hall-Petch (H-P) relation down to a grain size of 10 nm [5,14], whereas a negative H-P slope was observed below a grain size of 10nm [5]. It was suggested that dynamic creep might be responsible for the negative H-P curve in the absence of strain hardening. Such results of short-term creep tests for nano-nickel indicate an important role of grain boundary sliding and diffusion in the primary creep [5].

### 2. Experimental Procedure

The sheets of pure nano-nickel and nano-nickel doped with 700 wt ppm boron (nano Ni-700B) were prepared by pulse electrodeposition technique at the Integran Technologies Inc. The sheet material has full density, an average grain size of 30 nm and a thickness of 0.3 mm. The main impurities, carbon and sulphur, have been determined to be 500 ppm and 300 ppm respectively. Tensile and creep specimens with 15 mm gauge length and 3 mm gauge width were cut by an electron-discharge machine (EDM). The tensile tests were carried out by a MTS-810 Material Test System under stroke control condition at an initial strain rate of  $4 \times 10^{-5} \text{ s}^{-1}$ . A high sensitivity extensometer was attached to the gauge section of the specimens to measure displacement. Both load and displacement signals were digitized

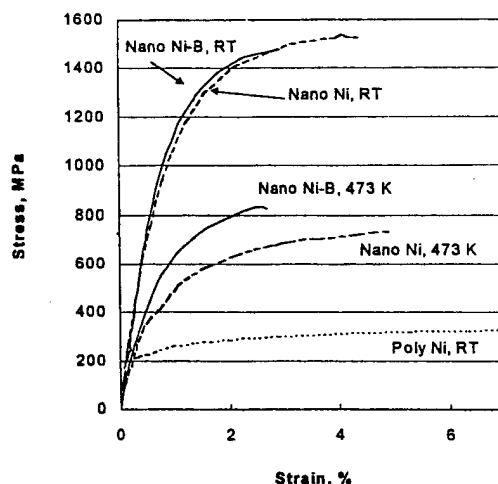


Figure 1. Effect of Boron on tensile behavior of nanocrystalline Nickel.

by 195A Keithley digital multimeters and recorded using a Personal computer equipped with an IEEE-480 board.

The uniaxial creep tests were performed at room temperature, 373K and 473 K in the load range of 200-1000 MPa using a Satec M3 creep machine. The step-load method was employed to exploit creep rate change and instantaneous deformation behavior during loading and unloading. TEM foils were cut by EDM from the as-received sheets as well as from the deformed specimens. The final polishing was prepared by double-jet electropolishing in a solution of 25%  $\text{HNO}_3$  and 75%  $\text{CH}_3\text{OH}$  at 220K and 30V. The x-ray line broadening technique was used to determine the average grain size.

### 3. Results

#### 3.1. Tensile Tests

The average grain size determined by x-ray line broadening technique was found to be approx. 30 nm. The results of tensile tests on nano-nickel, nano Ni-700B and polycrystalline nickel with 30  $\mu\text{m}$  grains are compared to each other in Fig. 1. The 0.2% offset engineering strength for nano-nickel and nano Ni-700B is as high as 1 GPa while that of polycrystalline nickel is about 300 MPa at room temperature. The effect of boron doping on yield strength is negligible at this temperature. Nevertheless, the ductility in both nano-nickel and nano Ni-700B is approx 2-4% at a strain rate of  $4 \times 10^{-5}/\text{s}$ . The trade-off for the high strength in these nano-materials is ductility reduction. The tensile strength of both materials, however, exhibits a divergence, showing sensitivity to temperature as shown in Fig. 1. At 473K, the 0.2% offset strength was approx. 400 MPa for nano-nickel and approx. 600 MPa for nano Ni-700B. The deviation between the two tensile curves increases with increasing strain (Fig. 1). It also shows that the elongation of nano Ni-700B decreased at 473K whereas that of pure nano-nickel increased at the same temperature. For nano-nickel, the initial slope, the stress/strain ratio significantly decreased at 473 K, which indicates that plastic deformation progress further at this temperature. Nano Ni-700B was pre-heat treated at 473 K for 5 h before tensile testing. The test results show some interesting contrast between the treated and untreated alloys shown in Fig. 2. The heat-treated nano Ni-700B shows higher stiffness and lower elongation than the untreated nano Ni-700B.

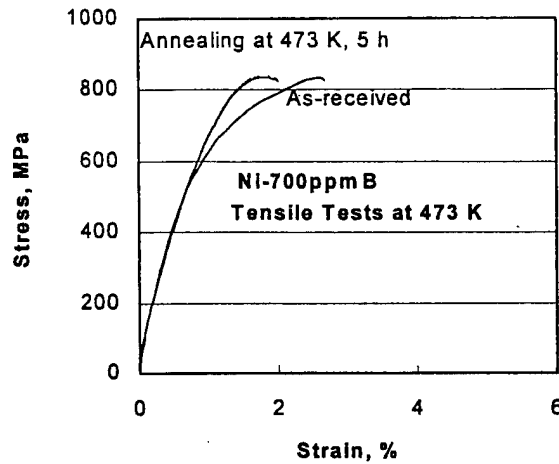


Figure 2. Effect of annealing on tensile behavior of nanocrystalline Nickel doped with Boron.

### 3.2. Creep Behavior

Creep testing on nano Ni-700B was conducted at room temperature and 373 K. The results are shown in Fig. 3. One characteristic feature is that the creep rate changes drastically from room temperature to 373 K. The prolonged primary creep was observed at 373 K and 600 MPa; and the corresponding minimum creep rate was achieved after approx. 70 h. The minimum creep rate at room temperature was less than  $10^{-9} \text{ s}^{-1}$ . It is important to note that the creep in this material is ultra-sensitive to temperature as demonstrated in Fig. 3, where the creep rate increased by many orders of magnitude as the temperature was raised only by 100K. To understand the creep mechanism better, the creep test at 373 K was interrupted after the primary creep was established. The load was removed from the specimen for a while so that the specimen recovered from elastic and anelastic deformation. Figure 4 shows the recovery process in the boron-doped nano-nickel after the load was removed at 373 K. The recovered elastic strain is slightly smaller than the instantaneous strain, i.e., approx. 82% of the instantaneous strain, and the remaining, approx. 18%, was recovered by an anelastic form. The anelastic recovery took place over a period of 20 h. The minimum creep rate of nano Ni-700B was compared with that of pure nano-nickel [7] in Fig. 5. The creep rate gap between the two materials become more pronounced with

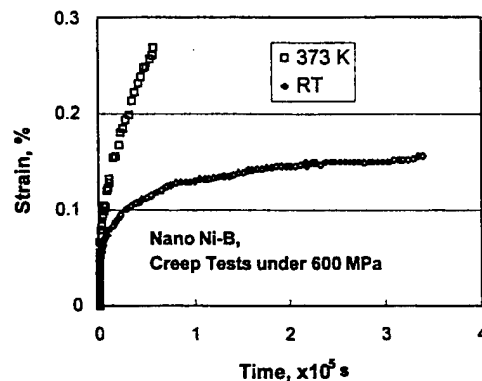


Figure 3. Creep behavior of nanocrystalline Nickel doped with Boron.

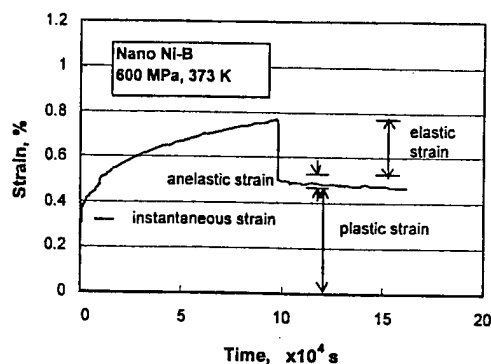


Figure 4. Anelastic behavior of nanocrystalline Nickel doped with Boron.

increasing temperature. In specific, the strain rates for both materials are nearly the same at room temperature, but the strain rate difference between two materials became a half order of magnitude at 373K, and an order of magnitude at 473K. The stress exponents determined from the curves were 2.2 at RT, 5.5 at 373K and 4.0 at 473K. The doping of a small amount of boron to pure nickel significantly reduces creep in this material.

#### 4. Discussion

##### 4.1. Tensile Strength

The tensile stress-strain curves for nano-nickel doesn't show a well defined linear elastic region, but an approx. value of Young's modulus 150 GPa was obtained from the initial slope in Fig. 1, which is somewhat lower than that of polycrystalline nickel 200GPa. This indicates that the lower value of nano-nickel may be attributed to the premature grain boundary sliding. The fact that the deformation is sensitive to the strain rate implies the existence of time-dependent deformation. Furthermore, with increasing temperature, the strain rate dependence becomes more pronounced.

A nanocrystalline material with a large volume fraction of the interfaces may be regarded as a composite consisting of crystalline components and various intercrystalline components. In nanocryst-

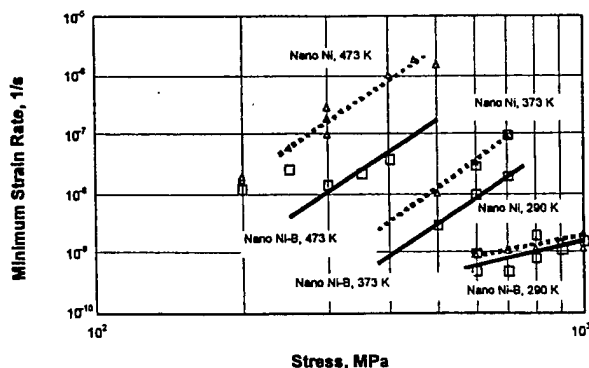


Figure 5. Minimum strain rate dependent on stress.

talline materials, the intercrystalline components include grain boundaries, triple lines and quadruple nodes. Therefore, the total strain in this material may be expressed as:

$$\epsilon_t = \epsilon_{el} + \epsilon_{dg} + \epsilon_{gs} \quad (1)$$

The term  $\epsilon_{el}$  is elastic deformation of crystalline components; and  $\epsilon_{dg}$  and  $\epsilon_{gs}$  are strains resulting from dislocation glide, and grain boundary sliding, respectively. To complete form of Eq. 1, each term of equation (1) must be defined with respect to temperature and grain size. The grain boundary migration is caused by grain boundary diffusion and sliding.

It has been suggested that there is no hardening effect in nanocrystalline materials at room temperature deformation [2,5]. This indicates that the dislocation pile-ups necessary for strain hardening may be absent or negligible in this material. Consequently, the grain boundary migration is the main mechanism for plastic deformation in such a material. Compared with impurities in nano-Ni, the boron-doped alloy showed a substantial strengthening with boron. Both materials exhibited randomly orientated grains with 30 nm dia. Therefore, the strengthening effect in nano Ni-B should be attributed to the grain boundary strengthening by boron. The role of boron in grain boundary sliding appears to be significant from current experiments. It is a known fact that boron and nickel forms a strong bond in grain boundaries, e.g., in  $\text{Ni}_3\text{Al}$  [15]. One of the plausible explanations is that such strong bond would provide resistance against grain boundary sliding.

#### 4.2. Creep Mechanism

It is interesting to investigate the origin of strain rate sensitivity since it may be related to a unique deformation mechanism such as migration and sliding of the intercrystalline components. In order to understand the stress dependence of creep deformation, the strain rate was plotted against stress from the constant load and step load tests (Fig. 5). The Norton stress exponent in Fig. 5 is 2.2 for room temperature creep while it is 5.5 for creep at 373K. In current experiments, no evident grain growth was found up to 373K.

The creep rate of diffusional Nabarro-Herring or Coble creep exhibits a linear dependence on true applied stress. In a material with small grain sizes, the grain boundary diffusion dominates over the lattice diffusion. Consequently, under these conditions, the diffusional creep will occur by stress directed mass transport through grain boundaries. Assuming spherical grains, Coble derived the following equation for creep rate [16]:

$$\dot{\epsilon} = \frac{148 D_b \delta_b \sigma \Omega}{\pi d^3 k T} \exp\left(-\frac{Q_b}{RT}\right) \quad (2)$$

where  $D_b$  is grain boundary diffusion coefficient,  $\delta_b$  is effective grain boundary width and  $\Omega$  is atomic volume. Since diffusion coefficient  $D_{i0}$  in nanocrystalline nickel is not available, the data for polycrystalline nickel, i.e.,  $\delta_b D_{b0} = 4 \times 10^{-15} \text{m}^3/\text{s}$  and  $Q_i = 108 \text{kJ/mol}$  [17] were used here. At room temperature and 600MPa, the calculated minimum strain rate  $2.8 \times 10^{-10}/\text{s}$  is of the same order of magnitude as the experimental value  $7.5 \times 10^{-10}/\text{s}$ . On the other hand, the stress exponent of 2.2 was obtained from the curves of minimum strain rate and stress at 273K. This indicates that the creep mechanism may no longer be governed only by the Coble mechanism, but possibly influenced by the dislocation mechanism.

## R-Curve characterization of the fracture toughness of nanocrystalline nickel thin sheets

R.A. Mirshams <sup>b,\*</sup>, C.H. Xiao <sup>a</sup>, S.H. Whang <sup>c</sup>, W.M. Yin <sup>c</sup>

<sup>a</sup> Mechanical Engineering Department, Southern University, Baton Rouge, LA 70813, USA

<sup>b</sup> Department of Engineering Technology, University of North Texas, P.O. Box 310679, Denton, TX 76203-0679, USA

<sup>c</sup> Mechanical Engineering Department, Polytechnic University, Six Metrotech Center, Brooklyn, NY 11201, USA

Received 15 August 2000; received in revised form 8 February 2001

### Abstract

The fracture resistance curves of nanocrystalline nickel and carbon doped nanocrystalline nickel for different annealing temperatures have been generated and studied. The results indicate that crack growth resistance of pure nanocrystalline nickel is very sensitive to annealing temperatures. The crack growth resistance decreased with increasing annealing temperature for the nanocrystalline nickel. Carbon doping greatly reduces crack growth resistance of nanocrystalline nickel. However, the crack growth resistance of carbon-doped nanocrystalline shows improvement through annealing processing. A cluster model was used to explain the crack growth resistance behavior of nanocrystalline nickel. © 2001 Elsevier Science B.V. All rights reserved.

**Keywords:** Nanocrystalline materials; Nickel; Fracture toughness; R-curve; Crack growth

### 1. Introduction

Nanocrystalline materials have been studied for their attractive properties for more than a decade. Gleiter [1] and Suryanarayana and Koch [2] reviewed and provided a comprehensive analysis for these materials. Cheung [3] also addressed their application. What differentiates these materials from their counterpart conventional is their grain structure. This difference in grain structure significantly alters some of the properties. As a result, many potential applications have emerged in areas such as magnetic, structural, catalysis, wear and corrosion materials. Meanwhile the processing methods and scale-up production technologies have also been developed for these materials. The most common preparation techniques for nanocrystalline metals and alloys are inert gas condensation (ICG), ball milling (BM) and pulsed electrodeposition (PED). Higher cost of production, ICG, and introduction of impurities and large elastic lattice distortions, BM, associated with some of these techniques, has left PED

as an attractive bulk production method for these materials.

The process, PED, has yielded a number of nanocrystalline pure nickel and nickel alloys [4]. Nanocrystalline materials processed by PED show controlled grain sizes between 10 and 100 nm. These materials are of high density and porosity-free. The strength of nanocrystalline electrodeposited Ni and Ni–P sheets far exceeds those of conventional Ni alloys with large grains and can be produced in thickness up to 600  $\mu\text{m}$  with grain sizes between 10 and 100 nm [5,6]. These materials exhibit excellent mechanical properties and great potential for structural applications [7,8].

The development of nanostructured materials is now raising the question of how the different properties change as the microstructural scale is reduced to nanometer dimensions. Traditionally the mechanical strength  $\sigma$  of crystalline materials is believed to be largely controlled by the grain size, often in manner described by the Hall–Petch relationship  $\sigma = k d^{-1/2} + \sigma_0$ . Although there are a lot of observations that follow the Hall–Petch relationship, observations by Erb and his co-workers [8] on the relationship of micro-hardness and grain sizes in the nanometer range pointed out that the Hall–Petch relationship may not be valid for

\* Corresponding author. Tel.: +1-940-5654961; fax: +1-940-5652666.

E-mail address: mirshams@unt.edu (R.A. Mirshams).



nanocrystalline metals. As the structural scale reduces to the nanometer range, the limits to conventional descriptions of yielding need to be established, and new mechanisms that may come into play at these very small dimensions need to be explored and studied.

Detailed works on the characterization of nanocrystalline material are required to realize their full potential. In particular, fracture toughness and creep resistance of these materials are of main concerns for long-term structural applications. Currently, the fracture mechanics theory in most micron grain size metals has established a solid foundation for reliable analysis of fracture toughness testing and has helped to understand the fracture mechanism in polycrystalline materials. However, studies of fracture toughness on nanocrystalline materials are very limited to date.

Previously, the mechanical properties of thin sheet nanocrystalline pure Ni, and carbon doped nanocrystalline nickel with different amount of carbon concentration from 500 to 1000 ppm at intermediate temperatures were reported at [9]. The purpose of this paper is to examine the fracture and fracture toughness and fracture resistance of these materials with different concentration of carbon and at different annealing temperatures.

## 2. Experimental procedures

### 2.1. Materials

The materials used in this research were two kinds of nanocrystalline nickel produced by an electrodeposition technique: pure nanocrystalline nickel (designated PRNi), 500 ppm carbon doped nanocrystalline nickel (designated CDNi). The materials have full density (pore free) and a narrow grain size range, which has been achieved by the precise control of electrical and chemical parameters [6]. The electrodeposited nanocrystalline materials were acquired from Integran Technologies Inc, Toronto, Canada. As a comparison, a commercial pure polycrystalline nickel (designated PLNi) was also used in this study. Table 1 presents a summary of properties tensile and hardness of nanocrystalline nickel from previous stage [9].

Table 1  
Mechanical properties of nanocrystalline nickel

Specimen	$\sigma_{UTS}$ (MPa)	$\sigma_{0.2\%}$ (MPa)	$\delta$ (%)	Hardness (HK)	Grain size (nm)
PRNi_as-received	1527	1307	2.25	463	19
PRNi_100°C annealed	1604	1324	2.20	455	21
PRNi_200°C annealed	1571	1283	2.20	470	25
CDNi_as-received	1140	904	0.5	491	18
CDNi_200°C annealed	1289	803	2.40	568	48
PLNi	366	299	35	122	21 ( $\mu\text{m}$ )

The grain size was determined from the calculation based on the broadening of the X-ray diffraction peaks. The lowest angle peak (111) was chosen for calculation. The X-ray measurements were conducted on a Philips Norelco 2-axis diffractometer with Jade analysis software. The crystalline grain size was estimated from the following formula [10]:

$$\text{Grain size} = \frac{0.9\lambda/\sqrt{B^2 - b^2}}{\cos\theta}, \quad (1)$$

Where  $\theta$  is half of the reported peak centroid,  $B$  is the reported peak width at half maximum in radians,  $b$  is the instrument's broadening and  $\lambda$  is the wavelength.

Scanning electron microscopy (SEM) was used to estimate grain sizes bigger than 100 nm for the samples tested at higher temperatures. A Hitachi SEM was used for this purpose. The etchant for microscopic examination consists of one part  $\text{HNO}_3$  (concentrated) and one part acetic acid.

The pole figures were obtained from Philips X'Pert MRD 4-axis X-ray diffractometer by tilting the specimen in reflection to a maximum of  $90^\circ$  in  $2^\circ$  angular intervals. For more detail refer to [9].

### 2.2. Tensile testing

Uniaxial tensile testing experiments were carried out to determine the basic tensile properties, yield strength, ultimate tensile strength, etc. Dog-bone shaped tensile test samples were water-jet machined to have a nominal gage section of  $25.4 \times 4$  mm. The thicknesses varied between 0.22 and 0.35 mm for pure nano nickel and carbon doped nano nickel, respectively. The tensile tests were carried out on a MTS 810 machine with a maximum 2500 kg load cell and TestStar™ II control system software. More details are described in the reference [9].

### 2.3. Fracture toughness experiments

Fracture toughness testing was performed using small compact tension specimens with dimensions of 32 (width) mm and 40 (height) mm. The thicknesses of specimens were 0.22 mm for pure nano nickel and 0.35 mm for carbon doped nano nickel. All specimens were machined by water jet machining. Subsequently, a wire

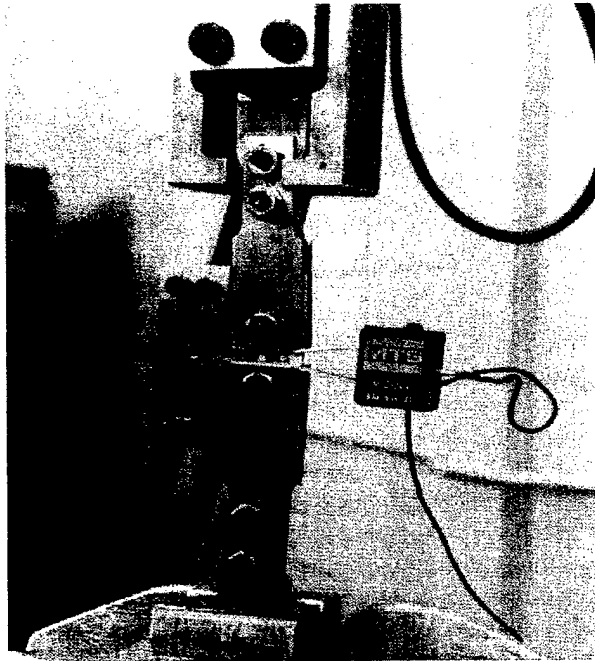


Fig. 1. The special designed fixture and setup for fracture toughness testing of the thin samples.

diamond saw was used to cut a slot with a root diameter between 0.15 and 0.20 mm.

All fracture toughness-testing samples were fatigue-precracked. Fatigue pre-crack was created in a tension–tension mode using a MTS810 servohydraulic machine. The processes were conducted under load control at a frequency of 15 Hz. The waveform was sinusoidal, and a constant stress ratio (minimum load/maximum load) of  $R = 0.1$  was maintained. A 2500 kg load cell was used for this purpose.

Fracture toughness testing was carried out per ASTM E561 Standard Test Method [11]. The crack length used in calculation of crack extension resistance,  $K_{Rc}$ , values is the effective crack length  $a_e$ , which is the total physical crack length plus a correction for plastic zone,  $r_Y$ . Correct physically measured crack lengths as follows:

$$a_e = (a_0 + \Delta a_p + r_Y),$$

where:  $a_0$ , original crack length;  $\Delta a_p$ , physical crack growth at one crack tip;  $r_Y$ , plastic-zone adjustment  $r_Y = (1/2\pi)(K_{Rc}^2/\sigma_Y^2)$ ;  $\sigma_Y$ , yield strength.

A special designed anti-buckling fixture was used for holding the specimens. Fig. 1 shows the fixture and setup for fracture toughness testing. G-n Metal Assembly Paste (a lubricant made by Dow Corning Corporation) was placed around the specimen to reduce friction. Steel washers were used to prevent lateral motion of the specimen at the loading-pin holes. A clip-on gage was used to record crack opening displacement. The crosshead speed was kept at  $0.03 \text{ mm min}^{-1}$ . Crack propagation was monitored and measured optically with a traveling microscope. Two identical samples were tested for each condition. The reported values are averages of two experiments.

### 3. Results and discussion

The resulting loads vs. crack mouth opening behavior are given in Fig. 2. It is noted that all the specimens initially exhibited linear elastic behaviors. However,

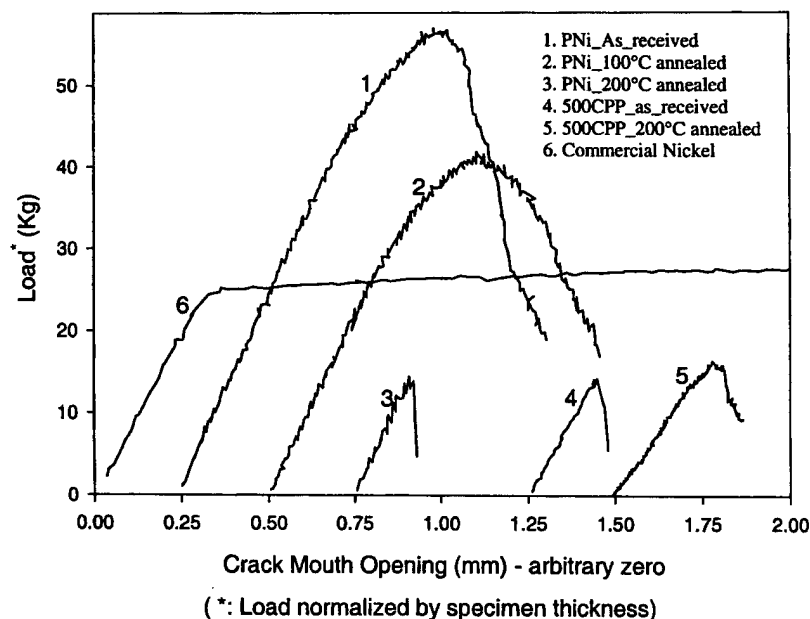
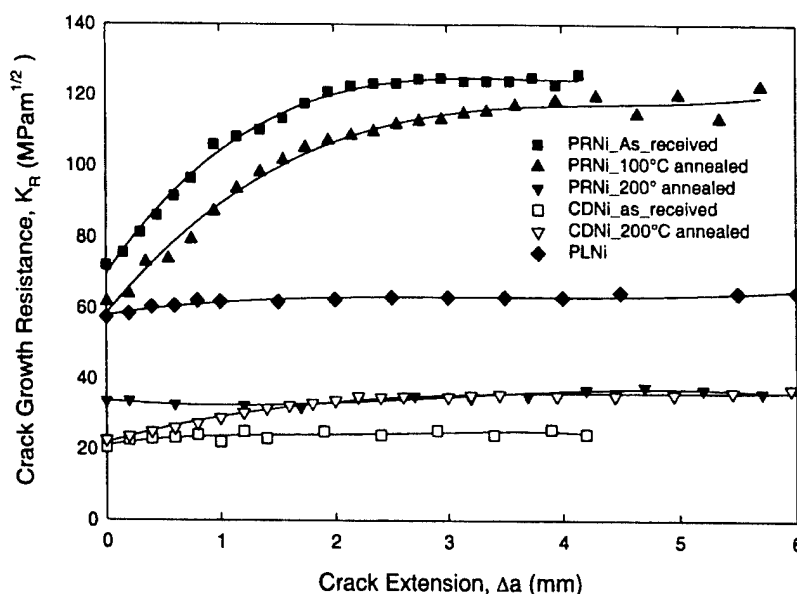


Fig. 2. Load – crack mouth-opening curves (\*: load normalized by specimen thickness).

Fig. 3.  $K_R$ -resistance curves.

only PRNi\_200°C annealed and CDNi\_as-received keep linearity until loads drop. All the others became nonlinear with increasing loads. The non-linearity was an indication of crack-tip plastic flow and stable crack growth. After the linear part of PLNi, it presents a nearly flat plastic-flow.

Fig. 3 presents a comparison of the  $K_R$ -resistance curves of the materials. As shown in Fig. 3, there are two kinds of the  $K_R$  curves. One is flat with zero slopes and the other has non-zero slopes. The initial fracture toughness values  $K_R$  for pure nanocrystalline nickel in as-received, 100°C annealed and 200°C annealed are about 72, 62 and 34  $\text{MPa m}^{1/2}$ , respectively and 62  $\text{MPa m}^{1/2}$  for polycrystalline nickel. Once start, subsequent crack extensions in the as received and 100°C annealed nickels were stable and showed higher crack growth resistances than that of polycrystalline nickel. This was indicated by the rising resistance curves in Fig. 3 and the nonlinear parts of the mouth opening curves in Fig. 2. In contrast, for the 200°C annealed pure nanocrystalline nickel, crack propagated unstably under a constant  $K_R$  level, leading to a zero slope in the  $K_R$ -resistance curve. These results indicate that fracture toughness resistance for pure nanocrystalline nickel is very sensitive to the annealing temperature. Its fracture toughness decreases with increasing annealing temperature. In other word, its thermal stability is poor. Although annealing slightly changed the  $K_R$  values for CDNi (carbon doped nickel), the shapes of  $K_R$  curve were changed from zero slope (unstable crack growth) to non-zero slope (stable crack growth). Therefore, it could be concluded that the annealing could improve the  $K_R$ -resistance of carbon doped nanocrystalline nickel. This also indicated that carbon doping might improve the thermal stability for nanocrystalline nickel.

However, carbon doping strongly reduces  $K_R$ -resistance of nanocrystalline nickel.

Fig. 3 shows that polycrystalline nickel exhibits a flat  $K_R$  curve, but its fracture was not stable. When a slope of  $K_R$  curve is zero, its load – crack mouth opening curve should be also used to determine whether a fracture is stable or unstable. In this case, the crack tips of polycrystalline nickel stably extended under a constant load (flat plastic-flow, Fig. 2) and a constant  $K_R$  value.

After fracture toughness testing, all specimens necked through the thickness in varying extent. An example is shown in Fig. 4. The modes of fracture were a shear-dominant mode and there was not a significant change as a function of various heat treatments. Fig. 5 shows that PRNi sheet exhibits a typical ductile fracture mode for the as received, 100 and 200°C annealed. A trans-granular-tearing mode is prevalent for all of them. The difference among them is that the dimples are finer and

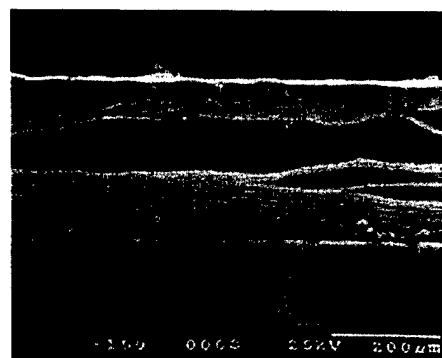


Fig. 4. A typical SEM fractograph of cross section over view in a fracture surface for as received nanocrystalline Ni. The figure shows a shear dominant mode of fracture.

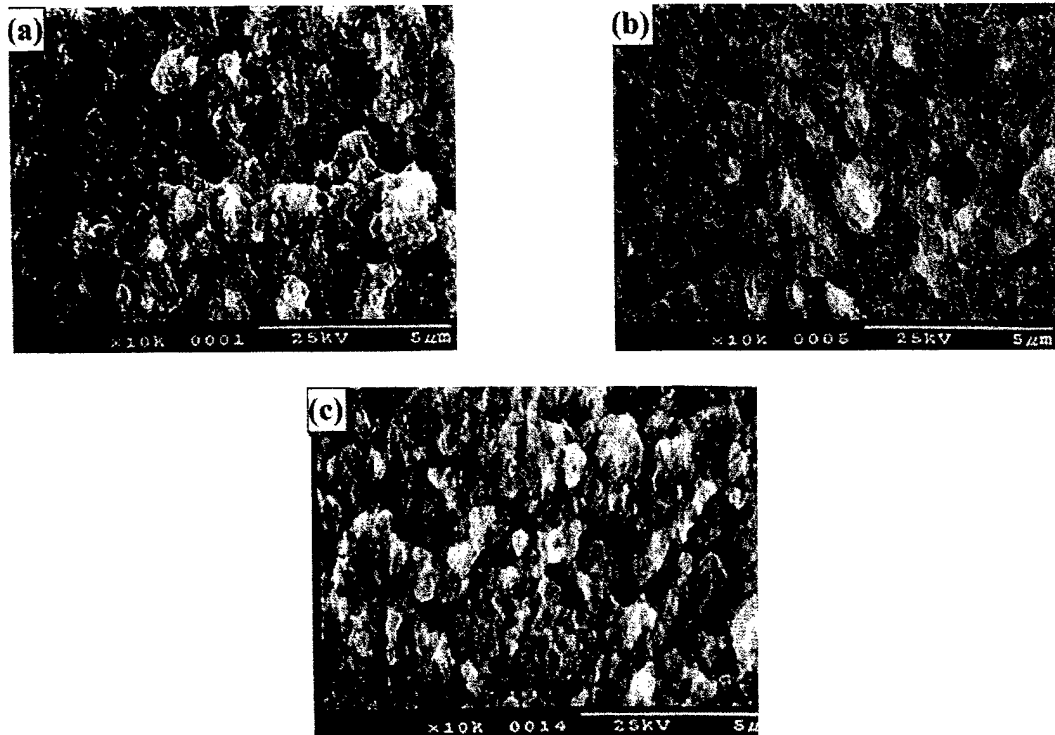


Fig. 5. SEM fractographs of PRNi: (a) as-received; (b) 100°C annealed; (c) 200°C annealed.

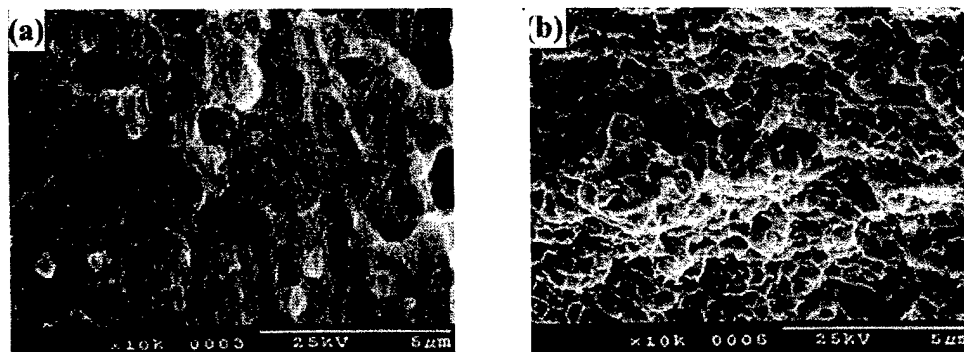


Fig. 6. SEM fractographs of CDNi: (a) as-received; (b) 200°C annealed.

deeper for the as-received (Fig. 5a), coarser for the 100°C annealed (see Fig. 5b), coarser and shallower for the 200°C annealed (Fig. 5c). These differences exhibited on fractography correspond to the difference of  $K_R$ -curves. For the carbon-doped nickels, the fracture surfaces also exhibited ductile fracture features with coarser dimples than those of pure nickel. For the as-received CDNi, the dimple size is relatively large and non-uniform (Fig. 6). The dimple shape is striped-tabular and elongated along the thickness direction of material. After annealed at 200°C, its dimple shape changes to spherical and uniform.

It is apparent that the crack growth resistance of pure nanocrystalline nickel is reduced with increasing annealing temperature. The exact reasons for this behavior are presently unknown. However, a cluster

model as proposed by Trusov et al. [12] can be used to explain the  $K_R$  behavior of nanocrystalline nickel in this research. According to this model, a large concentration of non-equilibrium vacancies is formed inside grains and at grain boundaries during the process of recrystallization of nanocrystalline materials. The physical reason for the high supersaturation was proposed to be the athermal emission of vacancies from grain boundaries dislocation during boundary migration [13]. The driving force for this process was proposed to be the reduction of the total free energy of the system due to grain growth. These dynamic vacancies are condensed into microvacancied clusters, which have been found to exist by experiments [14,15]. These clusters increase with increasing annealing temperature and preferentially segregate along grain boundaries. This

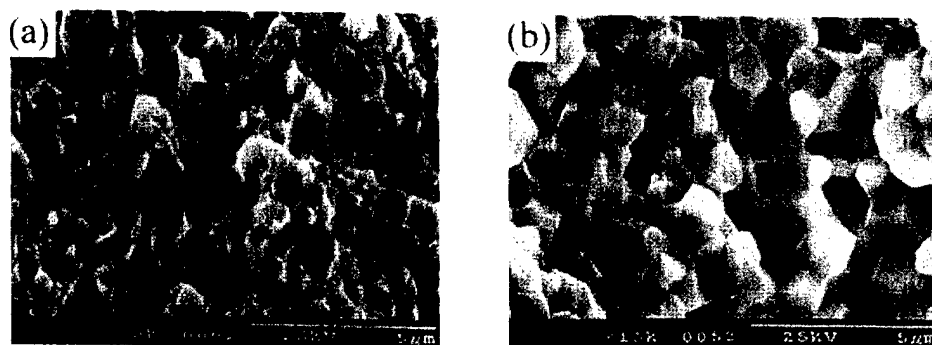


Fig. 7. SEM fractographs of PRNi after annealed at: (a) 300°C; (b) 500°C.

process would result in weakening grain boundaries and reduce the  $K_R$  properties of nanocrystalline materials. As the annealing temperature further increases to a higher level, except for grain growth the clusters would accumulate to grow up and even to form pores along grain boundaries, which significantly weakens the grain boundaries. When the grains grow up to micron level size, the fracture features of pure nanocrystalline nickel appeared to be totally intergranular fracture. Fig. 7a shows a mixture fracture mode with both transgranular ductile fracture and intergranular fracture for pure nanocrystalline nickel when it was annealed at 300°C. When the specimen annealed at 500°C, only intergranular fracture was observed. Fig. 7b clearly indicates that the separation occurs at grain boundaries. Although evidence for the emission of non-equilibrium vacancies by migration boundaries has been presented in conventional polycrystals [16], this effect will be much stronger in nanocrystalline materials due to the initial large volume of grain boundaries. Conventional nickels have not shown sensitivity to annealing temperature.

To improve the thermal stability of nanocrystalline nickel, 500 ppm carbon was doped in the nickel. Under thermal equilibrium conditions, carbon would preferentially segregate along the grain boundaries, which would reduce the grain growth. Furthermore, the doped carbon at grain boundaries might prevent the vacancies from segregating, or to reduce the segregation rate, or even to absorb the vacancies if the carbon segregates upon vacancy clusters. The reduction of the sensitivity to the annealing temperature of nanocrystalline nickel and improve  $K_R$  properties at higher annealing temperature (Fig. 3) could be related to this phenomenon.

#### 4. Summaries

(1) For pure nanocrystalline nickel, the crack growth resistance is very sensitive to annealing temperatures. The crack growth resistance decreased with increasing annealing temperature. When pure nanocrystalline

nickel was annealed at 100°C, it exhibited a stable crack growth and higher crack growth resistance than that of polycrystalline nickel. When it was annealed at 200°C, however, it showed an unstable crack growth and lower crack growth resistance than that of polycrystalline nickel.

(2) Carbon doping greatly reduced crack growth resistance of nanocrystalline nickel. However, the crack growth resistance of carbon-doped nanocrystalline nickel could be improved through annealing processing.

A cluster model as proposed by [12] can be effectively used to explain the crack growth resistance behavior of nanocrystalline nickels.

#### Acknowledgements

The authors would like to thank Dr Lawrence Kabacoff at the Office of Naval Research for financial support to complete this research under grant N0014-98-0666. Special thanks to Dr Parviz Razi for his assistance in  $K_R$  calculation.

#### References

- [1] H. Gleiter, *Prog. Mater. Sci.* 33 (1989) 223.
- [2] C. Suryanarayana, C.C. Koch, in: C. Suryanarayana (Ed.), *Non-equilibrium Processing of Materials*, Pergamon, 1999, p. 313.
- [3] C. Cheung, G. Plumbo, U. Erb, *Scripta Met.* 31 (1994) 735.
- [4] C. Cheung, D. Wood, U. Erb, in: S.J. Singh, F.H. Fores (Eds.), *Processing and Properties of Nanocrystalline Materials*, The Minerals, Metals & Materials Society, 1996, p. 479.
- [5] A.M. El-Shrik, U. Erb, J. Page, *Surface and Coatings Technol.* 88 (1996) 70.
- [6] A.M. Alfanzi, J. Page, U. Erb, *J. Appl. Electrochem.* 26 (1996) 1225.
- [7] B.H. Kear, G. Skandan, *Nanostructured Mater.* 7 (1996) 913.
- [8] U. Erb, G. Plumbo, R. Zugic, K.T. Aust, in: S.J. Singh, F.H. Fores (Eds.), *Processing and Properties of Nanocrystalline Materials*, The Minerals, Metals and Materials Society, 1996, p. 93.
- [9] C. Xiao, R.A. Mirshams, S.H. Whang, W.M. Yin, *Mater. Sci. Eng. A* 301 (1) (2001) 35.
- [10] Software Jade 3.1 Manual, XRD Pattern Processing for the PC, Materials Data, Inc., 1997.

- [11] Annual Book of ASTM Standards, vol. 03.01, ASTM, Philadelphia, PA, 1995, p. 492.
- [12] L.I. Trusov, V.G. Gryaznov, Growth of crystals, Consultants Bureau, New York and London, 1991, p. 55.
- [13] V.I. Novikov, V.Y. Ganelin, L.I. Trusov, V.G. Gryaznov, V.P. Lapovok, S.E. Zeer, Solid State Phys. (in Russian) 28 (1986) 1251.
- [14] V.P. Lapovok, V.Y. Ganelin, S.V. Svirida, A.N. Semenikhin, L.I. Trusov, Solid State Phys. (in Russian) 25 (1983) 1846.
- [15] L.I. Trusov, T.P. Khvostantseva, V.A. Soloven, V.A. Melnikova, J. Mat. Sci. 30 (1995) 2956.
- [16] C. Gottschalk, K. Smidoda, H. Gleiter, Acta Metall. 28 (1990) 1653.

# Effect of Interstitials on Tensile Strength and Creep in Nanostructured Ni

W. M. Yin<sup>a</sup>, S. H. Whang<sup>a</sup>, R. Mirshams<sup>b</sup> and C. H. Xiao<sup>b</sup>

<sup>a</sup>Department of Mechanical Engineering, Polytechnic University

Six Metrotech Center, Brooklyn, NY 11201

<sup>b</sup>Department of Engineering Technology, University of North Texas,

P.O. Box 310679 Denton, TX 76203-0679

Abstract: Nanostructured nickel with grain size 30 nm that was produced by the pulse electrodeposition method contains sulfur as an impurity. The concentration of sulfur varies from one deposition batch to another. Tensile tests were conducted with three different nanostructured nickel sheets containing sulfur 0.03 at %, 0.061 at % and 0.122 at %, respectively. The tensile strength is not sensitive to the sulfur content at room temperature while Ni-0.061 at % S exhibited the ultimate strength at 473 K that is 150 MPa higher than that of Ni-0.03 at % S. With increasing sulfur content in nanostructured Ni, the ductility decreases, indicating that the plasticity mainly depends on grain boundary sliding, and at the same time, the dislocations activity is very limited in this grain size. On the other hand, the creep results show that both minimum creep rate and creep strain significantly decrease with increasing sulfur content similar to the effect of boron on creep of nanostructured nickel. The Norton exponent increased to 6- 6.5 at 373 K in contrast to that of unity at room temperature.

## I. INTRODUCTION

Since the mid-1980s, increasing attention has been paid to nanostructured materials due to their unique mechanical, physical and chemical properties [1-4]. Although the majority of research work has been conducted in the areas of synthesis and processing, the preparation of nanostructured bulk materials of porosity-free has been proven to be

difficult. As a result, limited investigation on mechanical behavior including tensile fracture and creep has been carried out until now. In nanostructured nickel, the grain size effect on yield strength was interpreted using the Hall-Petch theory up to the grain size of 10 nm [5,6] whereas so called “negative Hall-Petch relation” was observed below grain size less than 10 nm [5]. It is suggested that the dynamic creep deformation might be responsible for the observed anomalous yield strength. The creep tests for nanostructured nickel confirmed an important role of grain boundary migration in the primary creep, though the detailed mechanism is not well known [5].

The tensile strength and creep of nanostructured materials strongly depend on two factors: grain size and grain boundary chemistry. Nanostructured Ni-P alloys showed improved strength due to the enhanced grain boundary binding by phosphorus segregation and/or precipitates like  $\text{Ni}_3\text{P}$  [7]. Recent study on boron doped nanostructured Ni showed that the boron doping not only enhances the tensile strength, but also increases the creep resistance [8]. Numerous experimental results suggest that the deformation behavior is sensitive to the segregation of metalloids at grain boundary in nanostructured nickel. In this paper, we examine the effect of sulfur on tensile and creep behavior in nanostructured nickel.

## II. EXPERIMENTAL PROCEDURE

Three different batches of nanostructured nickel sheets that were prepared by the pulse electrodeposition technique were obtained from Integran Technologies Inc. The nanostructured nickel that were produced by the pulse electrodeposition technique is free from pores, voids, or oxides and thereby, posses fully density with relatively uniform grain sizes [9]. Such a relatively micro-defect-free structure minimizes the uncertainty in



the mechanical testing and its results. The thickness of the sheets varied from batch to batch between 0.25 mm to 0.4 mm. LECO Combustion Analyzer was employed to analyze the concentrations of carbon and sulfur in nickel. The results were listed in Table 1. The other impurities specified by the producer were Si<75ppm, Cu<25ppm, Co<50ppm, Pb<2ppm which remained constant from one batch to another. In the present paper, we named the nano-Ni alloys from different batches: Ni-LS for low concentration of sulfur, Ni-MS for medium sulfur concentration and Ni-HS for high sulfur concentration.

Specimens for tensile and creep test were cut from the sheet material by electron-discharge machining. Each specimen has gauge dimensions of 15 mm in length 3 mm in width. The tensile tests were carried out on MTS-810 Material Test System under the stroke control condition at the initial strain rate of  $4 \times 10^{-5} \text{ s}^{-1}$ . A high sensitivity extensometer was attached to the gauge section of specimens to monitor the displacement. Both load and displacement signals were digitized by 195A Keithley digital multimeters and recorded using a PC computer with an analog-digital conversion board.

The uniaxial creep tests were performed under the stress range of 50MPa to 1GPa at room temperature, 373 K and 473K, respectively. The step-load method has been adopted to exploit creep rate change and instantaneous response during loading and unloading. Thin foils for TEM were cut by EDM from the as-received sheets as well as tested specimens. The final polishing was prepared by double-jet electropolishing in a solution of 25%  $\text{HNO}_3$  and 75%  $\text{CH}_3\text{OH}$  at 220K and 30V. Also, the grain size was determined

by X-ray line broadening technique. The microstructure of as-received materials and crept samples was investigated by TEM.

## RESULTS AND DISCUSSION

### A. Grain Boundary Segregation

Nanostructured nickel sheets shown in Fig.1 did not display any visible difference in appearance from the polycrystalline nickel. The x-ray diffraction patterns from the as-received nanostructured nickel sheets showed the line-broadening while the unusual peak strengthening associated with deposition texture was absent in the patterns. According to the Scherrer's formula, the grain size was determined from the broadened x-ray peaks and the three batches of nano-Ni used for current experiments showed approximate grain size of 30 nm. The bright-field TEM images of nano-Ni-MS showed relatively uniform equiaxed grains as showed in Fig. 2. Although the nano-nickel of porosity-free is advantageous for consistent data acquisition, the nano-nickel produced by electrodeposition method is contaminated with impurities such as S, C which were introduced from the bath solution during deposition. In our materials, the dominating impurities were carbon and sulfur, mainly coming from the additive saccharin. From Table 1, it can be found that the carbon concentrations of three materials remained almost same level whereas sulfur concentration varied from 0.03 at % to 0.122 at %. Obviously, these impurities tend to segregate to grain boundaries above room temperature during creep testing. Therefore, it is desired to calculate the equilibrium concentration of these elements at grain boundaries in order to understand the effect of these impurities on the deformation mechanism in nanostructured metals.

A general theory of interfacial segregation was developed on the basis of thermodynamic equilibrium for the distribution of different types of species between bulk and interface [10]. For a multicomponent system, the mole fraction of a particular interstitial at the interface may be written [11]:

$$\frac{X_I^\phi}{X^{0\phi} - \sum_J^{M-1} X_J^\phi} = \frac{X_I}{1 - \sum_J^{M-1} X_J} \exp\left(-\frac{\Delta G_I}{RT}\right) \quad (1)$$

where  $X_I^\phi$  and  $X_I$  are the mole fractions of element I at the interface  $\phi$  and in the bulk, respectively, and  $\Delta G$  is free energy of segregation. When the total concentration of impurities is extremely low, the above equation may be further simplified:

$$X_I^\phi = X_I \exp\left(-\frac{\Delta G_I}{RT}\right) \quad (2)$$

Further the concentration of impurities at grain boundary and inside grain can be calculated if the following relation is valid:

$$X_I^\phi V_{GB} + X_I(1 - V_{GB}) = X \quad (3)$$

where  $V_{GB}$  is the volume fraction of intercrystalline component, and  $X$  is the average concentration of a solute in the metal. The free energy of segregation is approximately equal to the segregation enthalpy as the segregation entropy may be very small. For the calculations of the concentration of sulfur at the grain boundary, the segregation enthalpy of sulfur in nickel,  $H=70\text{kJ/mol}$  [12] was used. The volume of grain boundary  $V_{GB}$  was found to be nearly 5% for the uniform grain size of 30 nm of nano-nickel by assuming

that the grain boundary thickness is 0.5nm. In the current study, the calculated sulfur concentration at grain boundary was 2.48 at % in Ni-HS containing 0.122 at %S. The high volume of grain boundary in nanostructured materials dramatically increases the total solubility of sulfur, which is consistent with the absence of precipitates in Ni-HS. The full results on carbon and sulfur concentrations are listed in Table 2. In high purity nickel, nickel sulphide phase could be produced with sulfur as little as 0.0018 at % [13, 14] whereas a low melting eutectic of nickel-nickel sulphide was found to surround grain boundary in conventional polycrystalline nickel containing greater than 0.01 at % S[15]. Meantime, the presence of sulfur segregation at intercrystalline defects has been found in nanocrystalline nickel containing 0.29 at %S [16]. It was also noticed that the sulfur concentration fluctuated along grain boundary in the annealed samples. In addition, there were evidences that sulfur content was higher at triple junction (5.3 at %) than at grain boundary (3.3at %) [16]. The calculated grain boundary concentration of sulfur in Ni-HS is smaller than that were 3.3 at % in nickel containing 0.29 at %S. The real grain boundary concentration should be higher than the experimental result. Therefore the calculated segregation at grain boundary is well consistent to the experimental results.

#### B. Tensile Behavior

The tensile test results at room temperature in Ni-LS showed that the 0.2% offset yield strength reached 1GPa, the ultimate strength was close to 1.5GPa and its elongation was less than 1% (Fig.3). At 373K, the ductility did not change evidently compared with the tests at room temperature while the ultimate strength slightly decreased. When the test

temperature was increased to 473K, the ultimate strength in Ni-LS dropped dramatically to half of the value at 373K.

The strength in Ni-MS was less sensitive to the test temperature, as shown in Figure 4. Consequently, Ni-MS exhibited 150MPa higher in ultimate strength than Ni-LS, in which the same level of ultimate strength at room temperature and 373K. The ductility of Ni-HS was so poor that all tensile specimens were broken during loading. To avoid embrittlement of sulfur in conventional polycrystalline nickel, sulfur content has to be below 0.001 at % [13].

When an array of dislocations in a grain is subjected by an applied stress, the lead dislocation near the grain boundary will be subjected to a stress given by an expression [17]:

$$\tau_b = \sum_{j=1}^n \frac{Gb}{2\pi(1-\nu)(l_i - l_j)}$$

In this formula,  $l_i$  ( $l_j$ ) is the distance from dislocation  $i$  ( $j$ ) to the obstacle. The solution showed that the stress acting (back stress) on the leading dislocation near the grain boundary with  $n$  parallel dislocations was found to be approximately 450 MPa for  $n = 2$ , 825 MPa for  $n = 3$  and 1250 MPa for  $n = 4$ , respectively. The stress for four dislocations is higher than the yield stress, 1.0 GPa and therefore, any significant pile-up of dislocations is practically excluded in most grains except much larger grains. It is also true that the grain size distribution exists in this material, and therefore the average grain size can not be used for dislocation pile-up calculations. In larger grains, a dislocation pile-up may occur at a much lower stress level whereas dislocation nucleation may not occur in sufficiently smaller grains. If this is the case, a new question arises as to the source of plastic deformation beyond yield stress. The idea is that the grain boundary

sliding is a competing mechanism against dislocation mechanism. The grain boundary sliding may be carried out by a few plausible mechanisms. First, in the absence of lattice dislocation activity, the activity of grain boundary dislocations would be a logical subject to investigate relative to the other deformation mechanisms in nanostructured nickel. By comparing the stress unlocking the Frank-Read source  $\sim Gb/2l$  with the plasticity yield stress  $\sim Kl^{1/2}$  [18], the critical grain size for generation of grain boundary dislocations was estimated to be several nanometers. The stress-induced and original grain boundary dislocations might be expected to travel along the interface without penetrating the nanostructured volumes. For the coincidence site lattice model, the Burgers vectors of secondary grain boundary dislocations are only a fraction of those of lattice dislocations. This means that the critical stress for the migration of secondary grain boundary dislocations is much lower than that for the glide of lattice dislocations. Therefore, grain boundary dislocations could be active in nanostructured nickel and contribute to plastic deformation. It is not easy to identify dislocations under high resolution TEM in nanograins since many deformation dislocations may disappear during the preparation of thin TEM specimens. Second, when the grain boundary structure is disordered and its viscosity lies below a critical value where the viscous flow can occur under the applied stress, the viscous flow may be realized. The viscous flow mode may require thermal activation. The first and second modes may be capable of deforming material under static deformation testing. The relationship between stress and strain rate in viscous flow obeys  $\sigma = 3\eta\dot{\epsilon}$  [19], and viscosity is sensitive to temperature and to a lesser degree, to applied stress. Third, the material still can be deformed by grain migration mainly caused by diffusion. This mechanism has been well known to occur in polycrystalline metals

and alloys at relatively high temperatures. It has been suggested that there is no hardening effect in nanostructured materials at room-temperature deformation [5]. This indicates that the dislocation pile-ups necessary for strain hardening may be absent or negligible in this material. Consequently, the grain boundary sliding and migration is the main mechanism for plastic deformation in such a material. Therefore, the sulfur in grain boundaries would be responsible for pinning grain boundary dislocations and the reduction of viscous flow.

### C. Creep Behavior

The nano-Ni-LS exhibited a prolonged primary creep whose minimum strain rate reached  $3 \times 10^{-10} \text{ s}^{-1}$  after 100 hours under 600MPa at room temperature while the minimum creep rate of nano-Ni-MS at room temperature approached one third of that Ni-LS (Fig.5). The nano-Ni-HS showed a reduced creep strain and very short rupture life for all creep tests. The step-load creep tests showed that the minimum strain rates were proportional to the applied stress for the nanostructured nickel independent of sulfur concentration.

The creep resistance is very sensitive to testing temperature for all three nano-Ni alloys. Nanostructured Ni-MS alloy exhibited an accelerated minimum creep rate above room temperature. For example, the minimum strain rate at 600MPa reached  $6 \times 10^{-8} \text{ s}^{-1}$  at 373K, which is about two orders of magnitude larger than that at room temperature. The Ni-LS showed an even higher minimum creep rate, which was about  $8 \times 10^{-8}$  under 400MPa and 373K. At 473K, the minimum strain rate of the Ni-LS alloy under 50MPa reached the level of Ni-MS under 200MPa (Fig.6).

Fig.7 shows the strain dependence in minimum strain rate for a given temperature. At 373K, Norton exponents were about 6.5 and 6 for nanostructured nickel Ni-LS and Ni-

MS. Creep activation energy of Ni-LS and Ni-MS can be calculated to be 85kJ/mol and 107kJ/mol respectively.

The creep rate in diffusional Nabarro-Herring as well as Coble creep with respect to true applied stress exhibits linear dependence. The dislocation creep rate is practically independent of grain size, while the diffusional creep rate is inversely proportional to the second power of mean grain diameter when the diffusion mass transport occurs via the lattice; and to the third power of mean grain diameter when it occurs through grain boundaries.

At low homologous temperatures, the grain boundary diffusion in small mean grain diameters dominates over the lattice diffusion. Consequently, under these conditions, the diffusional creep will occur by stress directed mass transport through grain boundaries. Assuming spherical grains, Coble derived the following equation for creep rate [20]:

$$\dot{\epsilon} = \frac{148}{\pi} \frac{D_{b0} \delta_b \sigma \Omega}{d^3 k T} \exp\left(-\frac{Q_b}{RT}\right) \quad (7)$$

In the formula,  $D_b$  is grain boundary diffusion coefficient,  $\delta_b$  is effective grain boundary width and  $\Omega$  is atomic volume. Since diffusion coefficient  $D_{b0}$  in nanostructured nickel is not available, the data for polycrystalline nickel, i.e.,  $\delta_b D_{b0} = 4 \times 10^{-15} \text{ m}^3/\text{s}$  and  $Q_b = 107 \text{ kJ/mol}$  [21] were used here. Given  $\Omega = 8.0 \times 10^{-3} \text{ nm}^3$ ,  $d = 30 \text{ nm}$ ,

$$\dot{\epsilon} = \frac{4 \times 10^3 \sigma}{T} \exp\left(-\frac{12996}{T}\right) \quad (8)$$

At room temperature under 700 MPa, the calculated minimum strain rate ( $3.3 \times 10^{-10}/\text{s}$ ) is of the same order of magnitude as the experimental value ( $11 \times 10^{-10}/\text{s}$ ). But the calculated strain rate based on Eq.7 was much smaller than that of the experimental value at 373 K.



This indicates that the creep mechanism may no longer be governed by the Coble mechanism, but possibly by the dislocation mechanism.

In nanostructured materials, the activity of dislocations is very low because of nanoscale grain size. Therefore sulfur should have little effect on lattice dislocation since the concentration is dilute in the grains not mention to the diminished dislocation activity. Thus, the role of sulfur should be pronounced in the deformation at grain boundary, where the grain-boundary sliding and high diffusion occur. Current study shows the material with 0.06at% sulfur exhibited highest creep resistance. How can this small amount of sulfur generate such strengthening effect? The molecular dynamics simulations by the embedded-atom-method have been performed to study the segregation of phosphorus atoms to Ni grain boundary [22]. The results showed that phosphorus reduced the number of micro-voids near grain boundary which implied that the existence of phosphorus increases grain boundary cohesion. In addition, there was the oscillation of segregation energy near grain boundary, which indicated that the composition distribution is not uniform. The fluctuation of sulfur along grain boundary was confirmed by the high resolution electron microscopy observation in nanostructured nickel containing 0.29at% sulfur [16].

The phenomena of fluctuation can be interpreted using the modified “Disordered Atom Group” model of grain boundary [23, 24]. Ke proposed that the grain boundaries would consist of many disordered-atom groups which are separated by regions of good fit. It is reasonable to assume that the solutes tend to stay in the cores of disordered-atom groups as the cores have larger excess free-volume. From the plot of the segregation fluctuation along grain boundary [16], the zone with high sulfur content can be measured around 10

nm. It might be deduced that disordered-atom groups can link each other to form “loose zone” separated by “fit zones”. Since atoms in “fit zones” are arranged more regularly with less free volume, “fit zones” are more resistant to the applied stress. The “loose zones” may allow for one atom to glide over another under sufficient stress. Therefore the “loose zones” may contribute to grain boundary sliding. This requires a local displacement having components both parallel and perpendicular to the grain boundary. The solute atoms located in the core of “loose zones” can reduce free volume, and result in pinning effect. From this analysis, it is unnecessary to form a mono-layer of solutes. Instead, a minute amount of solute is enough for strengthening grain boundary.

#### IV. SUMMARY

1. The effect of sulfur on tensile strength was less obvious at room temperature, but pronounced at moderate temperatures. As temperature increases, the tensile strength dropped very rapidly in nanostructured nickel containing 0.03at%S whereas the Ni-0.061at %S material maintained high yield stress level at 473K.
2. The tensile creep tests showed accelerated minimum creep rate in nanostructured Ni-0.03at%S compared to the nano-Ni-0.061at%S.
3. Very poor ductility of Ni-0.122at%S indicates that high concentration of sulfur as calculated to be 2.5 at % at grain boundary is significant enough to hinder grain boundary sliding; and for the applied stress of 200-1000 MPa, and the temperature range of RT-373K, the contribution of lattice dislocations to the deformation appears negligible.

Acknowledgement: The authors thank the support of the Office of Naval Research for this project.

Table 1 Trace Concentrations of Interstitials in Nanostructured Nickel\*

Alloy	C**, at. %	S**, at. %
Ni-LS	0.045±0.012	0.03±0.002
Ni-MS	0.033±0.009	0.061±0.004
Ni-HS	0.045±0.003	0.122±0.003

\* Si<75ppm, Cu<25ppm, Co<50ppm, Pb<2ppm

\*\* LECO Combustion Analysis for Carbon and Sulphur, the average obtained from three tests

Table 2 Calculated Concentrations of Interstitials at Grain Boundary in Nanostructured Nickel

Alloy	C, at. %	S, at. %
Ni-LS	0.9 <sub>1</sub>	0.6 <sub>1</sub>
Ni-MS	0.6 <sub>7</sub>	1.2 <sub>4</sub>
Ni-HS	0.9 <sub>2</sub>	2.4 <sub>8</sub>

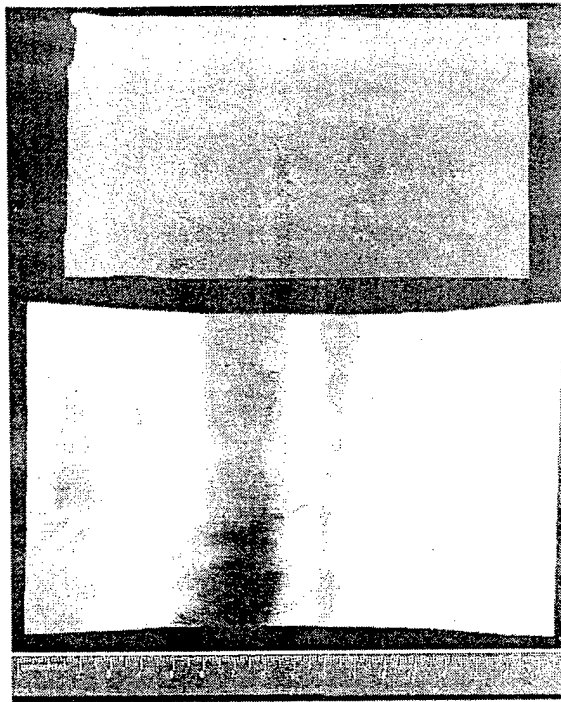


Figure 1 The as-received sheets of nanostructured nickel (top: Ni-LS, bottom: Ni-MS).

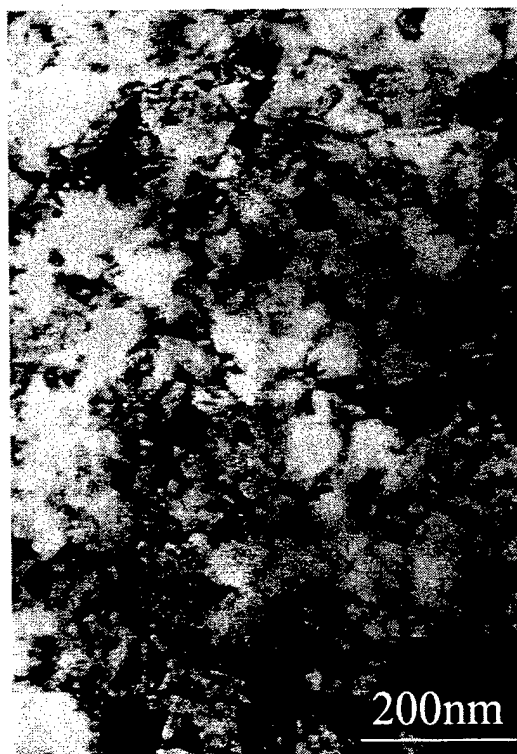


Figure 2 Bright field image of as-received nano-nickel (Ni-MS).

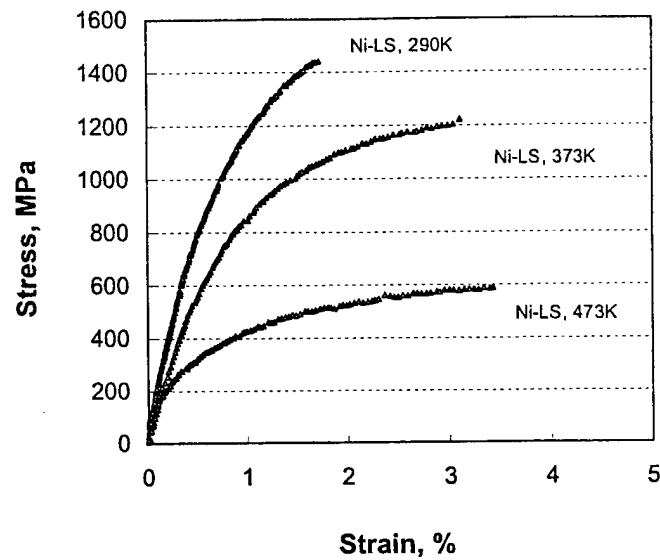


Figure 3 Tensile behavior of nanostructured Ni-LS.

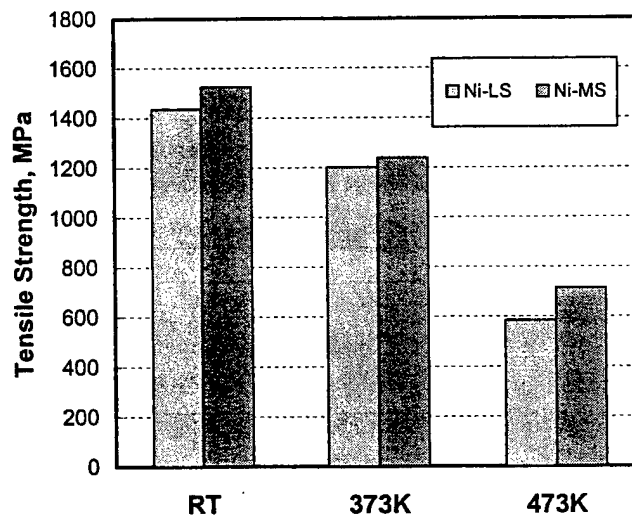


Figure 4 Effect of sulfur on tensile strength in nano-nickel.

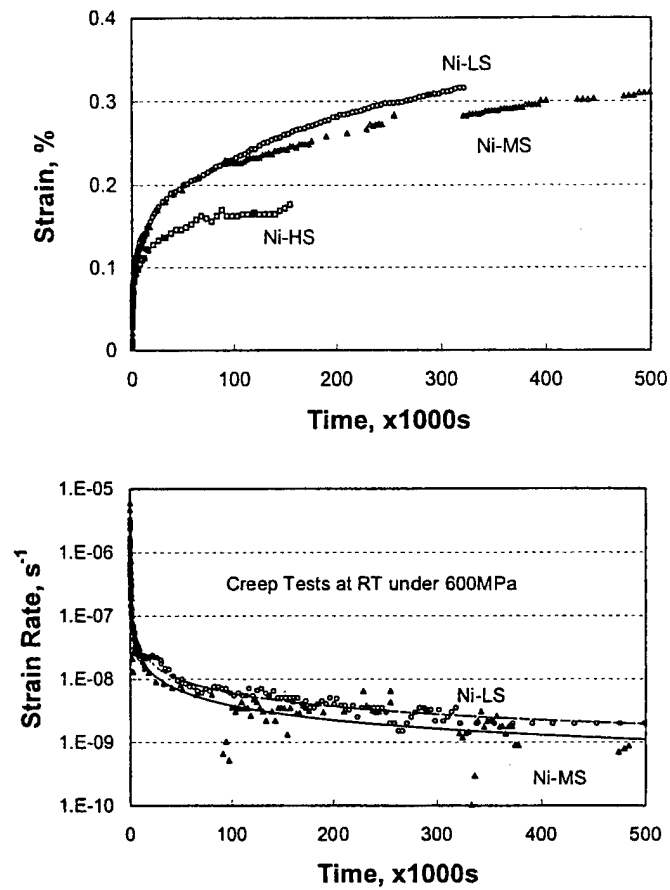


Figure 5 Creep behavior of nanostructured nickel at room temperature.

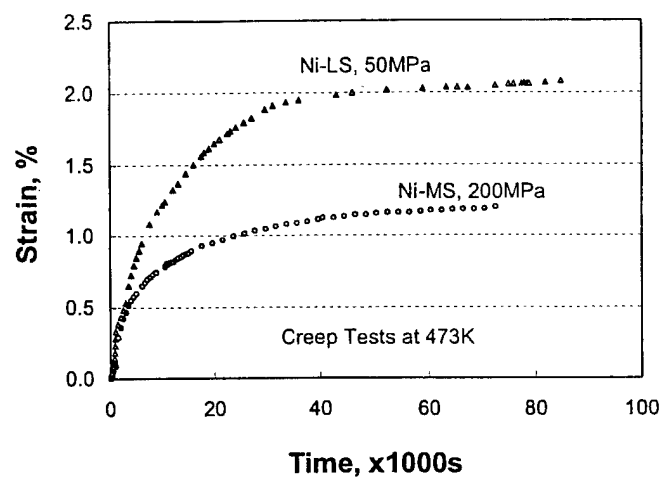


Figure 6 Creep behavior of nanostructured nickel at 473K.

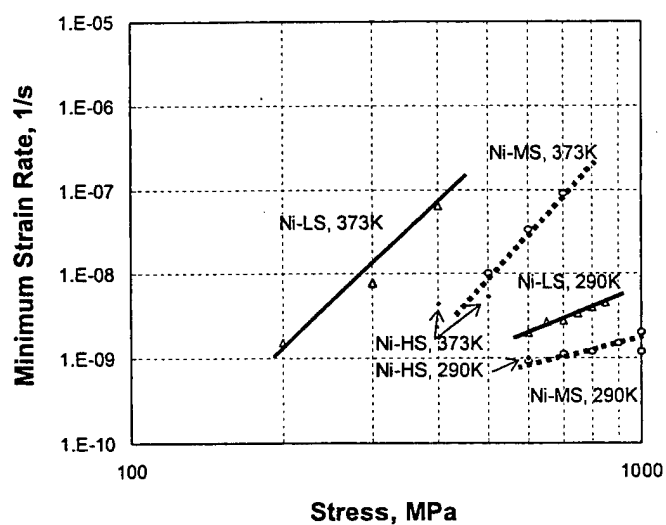


Figure 7 Minimum strain rate dependent on stress.

Figure 1 As-received sheets of nanostructured nickel: top: Ni-LS, bottom: Ni-MS.

Figure 2 Bright field image of as-received nano-nickel: Ni-MS.

Figure 3 Tensile behavior of nanostructured Ni-LS.

Figure 4 Effect of sulfur on tensile strength in nano-nickel.

Figure 5 Creep behavior of nanostructured nickel at room temperature.

Figure 6 Creep behavior of nanostructured nickel at 473K.

Figure 7 Plots of minimum strain rate vs. stress in three nickel alloys.



## References:

1. H. Gleiter: *Progress in Materials Science*, 1989, vol.33, pp. 223-315.
2. V.G. Gryaznov and L.I. Trusov: *Progress in Materials Science*, 1993, vol.37, pp. 289-401.
3. C.C. Koch, D.G. Morris, K. Lu, and A. Inoue: *MRS Bulletin*, 1999, vol.24 (2), pp. 54-58.
4. J. R. Weertman, D. Farkas, K. Hemker, H. Kung, M. Mayo, R. Mitra, and H. Van Swygenhoven: *MRS Bulletin*, 1999, vol.24 (2), pp. 44-50.
5. N. Wang, Z. R. Wang, K. T. Aust, and U. Erb, *Mater. Sci. Eng. A*, 1997, vol.237A, pp. 150-58.
6. F. Ebrahimi, G.R. Bourne, M.S. Kelly, and T.E. Matthews: *Nanostructured Materials*, 1999, vol. 11(3), pp. 343-50.
7. D.L. Wang, Q.P. Kong, and J.P. Shui: *Scripta Metall. Mater.*, 1994, vol. 31(1), pp. 47-51.
8. W.M. Yin and S.H. Whang: *Scripta Mater.*, 2001, vol. 44, pp. 569-74.
9. M. Alfantazi, J. Page, and U. Erb: *J. Applied Electrochemistry*, 1996, vol. 26 pp. 1225-34.
10. M. Guttman and D. McLean: *Interfacial Segregation*, W.C. Johnson and J.M. Blakely, eds., ASM, Metals Park, Ohio, 1979, pp. 261-68.
11. S. Hofmann and P. Lejcek: *Interface Science*, 1996, vol. 3, pp. 241-67.
12. K. Losch: *Ph.D Thesis*, University Stuttgart, 1987.
13. K.M. Olsen, C.F. Larkin, and P.H. Schmitt: *Trans. A.S.M.*, 1961, vol. 53, pp. 349-51.

- 
14. C.L. Lewis, W.L. Ott, and N.M. Sine: *The Analysis of Nickel*, Pergamon Press, London, 1966, 22-25.
  15. P.D. Merica and R.G. Waltenberg: *Bureau of Standards, Tech. Papers*, 1955, vol. 19, pp. 150-55.
  16. U. Klement, U. Erb, A.M. El-Sheik, and K.T. Aust: *Mater. Sci. Eng. A*, 1995, vol. 203A, pp. 177-86.
  17. E. Smith: *Dislocations and Cracks, in Dislocation in Solids*, F.R.N. Nabarro ed., 1979, vol. 4, pp. 374-76.
  18. A. Lasalmonie and J.L. Strudei: *J. Mater. Sci.*, 1986, vol. 21, pp. 1837-52.
  19. T.H. Courtney: *Mechanical Behavior of Materials*, McGraw-Hill Publishing Company, New York, NY, 1990, pp. 332-36.
  20. R.L. Coble: *J. Appl. Phys.*, 1963, vol. 34, pp. 1679-82.
  21. I. Kaur, W. Gust and L. Kozma: *Handbook of Grain and Interphase Boundary Diffusion Data*, Ziegler Press, Stuttgart, 1989, pp. 1014-45
  22. X. Liu, H. Liu, J. Dong and X. Xie: *Scripta Mater.*, 2000, vol. 42(2), pp. 189-95.
  23. T.S. Ke: *J. Appl. Phys.*, 1949, vol. 20, pp. 274-80.
  24. T.S. Ke: *Metall. Mater. Trans.A*, 1999, vol. 30A(9), pp. 2267-95.

# Ab-Initio Calculation for the Bond Formation in Ni-C Systems

By G. L. Zhao<sup>1</sup>, D. Bagayoko<sup>1</sup>, and R. A. Mirshams<sup>2</sup>

<sup>1</sup>Department of Physics, Southern University and A & M College,  
Baton Rouge, LA 70813

<sup>2</sup>Department of Mechanical Engineering, University of North Texas  
Denton, TX 76203

The tensile behavior and fracture properties of carbon doped nanocrystalline nickel systems has been studied by C. Xiao, R. A. Mirshams, S. H. Whang, and W. M. Yin.[1,2] These authors focused on carbon doped, face-centered cubic (fcc), nanocrystalline nickel systems. The dimensions of these systems varied from 10 to 100 nanometers. Grain growth was observed in the nanocrystalline nickel systems as temperature increased. A fast growth of the grains in nanocrystalline nickel samples was noticed at 300°C. The addition of carbon appeared to enhance the stability of the microstructures in the studied, nanocrystalline nickel systems at intermediate temperatures.

This computational research aims to understand some aspects of the microscopic mechanism driving the above behavior of carbon-doped, nanocrystalline, fcc nickel systems. In particular, we studied the formation, nature, and strength of the Ni-Ni and Ni-C bonds in these systems. In the first phase of this work, we performed ab-initio calculations for the electronic and magnetic properties, and the total energy versus the bond length for pure Ni and Ni-C alloy. We employed density functional theory, the linear combination of atomic orbitals (LCAO) formalism, and the Bagayoko-Zhao-Williams (BZW) procedure.[3-7] The total energy provides a measure of the formation energy and general stability of the system as the bond length changes. Further insight is expected from the comparison of the Ni-Ni and Ni-C bonds.

The calculated total energies for the formation of Ni-Ni bond and Ni-C bond are shown in Figure 1. In Figure 1, the zero energy is set at the total energy for the free atoms. In the calculation, the pure nickel phase is in the fcc structure. The Ni-C alloy is chosen in the zinc blend (ZB) structure, since the carbon atoms prefer four-fold coordination. For the pure fcc nickel phase, our calculated lattice constant is  $3.50 \pm 0.02 \text{ \AA}$ , which agrees very well with experimentally measured lattice constant of  $3.52 \text{ \AA}$ . [3] Our calculated magnetic moment from the spin polarization of nickel atom is  $0.57 \pm 0.01 \mu_B$  per atom. The experimentally measured magnetic moment of pure nickel is  $0.606 \mu_B$ . After allowance for the magnetic moment contribution from orbital magnetism, our calculated spin contribution agrees well with the published data of  $0.54 \mu_B$  per nickel atom.[3]

From Figure 1, we can see that the calculated minimum of the total energy of Ni-Ni bond is lower than that of Ni-C bond. This demonstrates that, in the carbon doped nickel nanocrystalline alloys, the formation of Ni-Ni bond is preferred to that of Ni-C bond. The nanocrystalline nickel grain has the tendency to attract the neighboring nickel

atoms. The calculated Ni-C bond length is  $1.88 \pm 0.02 \text{ \AA}$ , which is much shorter than the Ni-Ni bond length of  $2.47 \pm 0.02 \text{ \AA}$ .

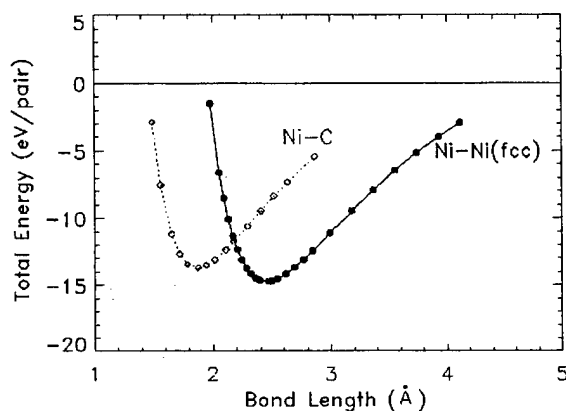


Figure 1. The calculated total energies for Ni-Ni and Ni-C.

In the growth of the nanocrystalline nickel grains, the neighboring coordinates of nickel atoms at the surface of a grain or at the interface of grains generally are different from that of the bulk fcc nickel. We have calculated the formation energies of the Ni-Ni bonds for the fcc nickel structure and for a zinc blend structure of pure nickel, as show in Figure 2. In the zinc blend structure of pure nickel, the Ni atoms are four-fold coordinated. Figure 2 shows the zinc blend structure of nickel is unstable, since the minimum of the total energy of Ni-Ni (ZB) is higher than that of Ni-Ni (fcc) bond at bond lengths over 2.2 Angstroms. Nickel atoms prefer the fcc structure with the twelve-fold neighboring coordinates. This behavior explains the growth of the nanocrystalline nickel grains in the face-centered cubic structure.

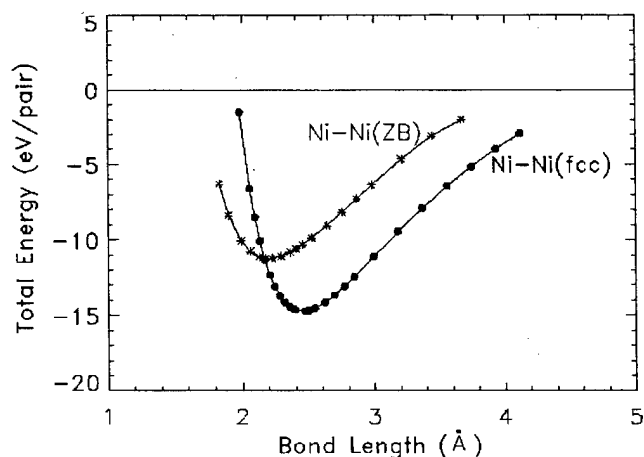


Figure 2. The formation energies of the Ni-Ni bonds for the fcc structure and for a zinc blend structure of pure nickel.

Future work of this project includes calculations of the formation energy of the chemical bonds of the nanocrystalline nickel systems with dopants other than carbon (i.e., boron, phosphorus, or nitrogen). The comparison of our results for the formation of the chemical bonds of Ni with different dopants is expected to shed light on the enhancement of the relative stability of carbon-doped nanocrystalline nickel systems. Future work also includes molecular dynamics (MD) simulations for the structural, dynamical, and mechanical properties of nanocrystalline nickel systems. From molecular dynamics simulations, we can calculate and even predict the structure factors of the materials that can be measured in various experiments. Molecular dynamics simulations can help us and other experimentalists to understand the growth process and the formation of various defects (such as voids, impurities, interstitial point defects, and dislocations) in nanomaterials. Such simulations will also provide the information regarding diffusion constant of percolation or doped atoms.

As well known, an appropriate potential of the inter-atomic interaction is the key to the success of a MD simulation. The input information of the inter-atomic potential will be derived from the ab-initio computations partly presented above. In that sense, a critical contribution of this work, in addition to the insights provided above, stems from the accuracy of the inter-atomic potentials derived from our ab-initio computational results.

### Acknowledgments

The authors wish to thank Dr. Lawrence Kabacoff, Program Officer, and the Department of the Navy, Office of Naval Research (ONR), for funding this work (Award No. N00014-98-1-0666).

### References

- [1]. C. H. Xiao, R. A. Mirshams, S. H. Whang, and W. M. Yin, "Tensile Behavior and Fracture in Nickel and Carbon Doped Nanocrystalline Nickel", accepted for publication in the J. of Mat. Sci. (2000).
- [2]. W. M. Yin, S. H. Whang, R. A. Mirshams, and C. H. Xiao, "Creep Behavior of Nanocrystalline Nickel at 290 K and 373 K", accepted for publication in the J. of Mat. Sci. (2000).
- [3]. G. L. Zhao and D. Bagayoko, "Electronic Structure and Charge Transfer in 3C- and 4H-SiC", *New Journal of Physics* **2**, 16.1-16.12 (2000), online 18 July 2000.
- [4]. G. L. Zhao, D. Bagayoko, and T. D. Williams, "Local-density-approximation prediction of electronic properties of GaN, Si, C, and RuO<sub>2</sub>", *Physical Review B* **60**, 1563 (1999).
- [5]. G. L. Zhao and D. Bagayoko, "Ab-Initio Calculations of Superconducting Properties of YBa<sub>2</sub>Cu<sub>3</sub>O<sub>7</sub>", *International Journal of Modern Physics B*, **13**, 3579 (1999).
- [6]. D. Bagayoko, G. L. Zhao, "Predictive Ab-Initio Computations of Properties of Ferroelectric Materials", *International Journal of Modern Physics B*, **13**, 3767 (1999).
- [7]. D. Bagayoko, G. L. Zhao, J. D. Fan, and J. T. Wang, "Ab initio calculations of the electronic structure and optical properties of ferroelectric tetragonal BaTiO<sub>3</sub>", *Journal of Physics: Condensed Matter*, **10**, 5645, (1998).
- [8]. C. Kittel, "Introduction to Solid State Physics, 7<sup>th</sup> Edition, (John Wiley & Sons, New York, 1996), Chapter 15.